https://doi.org/10.5194/egusphere-2026-3874
Preprint. Discussion started: 2 September 2026

Sea Level Emulator Intercomparison Project (SLEIP) Phase 1: Assessing emulated multi-century global mean sea level projections

Alexander Nauels[1,2], Tessa Möller[1,2,3], Victor Couplet[4], Robert E. Kopp[5,6], Praveen Kumar[5,6], Matthias Mengel[7], Gregory Munday[8], Zebedee R. J. Nicholls[1,2,9], Lennart Ramme[10], Aimée B. A. Slangen[11,12], Chris Smith[1], Jennifer H. Weeks[13,14], Tony E. Wong[15]

[1]International Institute for Applied Systems Analysis (IIASA), Laxenburg, Austria
[2]School of Geography, Earth and Atmospheric Sciences, The University of Melbourne, Parkville, Australia
[3]Geography Department, Humboldt-Universität zu Berlin, Berlin, Germany
[4]Earth and Life Institute, UC Louvain, Louvain-la-Neuve, Belgium
[5]Department of Earth and Planetary Sciences, Rutgers University, Piscataway, NJ, USA
[6]Rutgers Climate and Energy Institute, Rutgers University, New Brunswick, NJ, USA
[7]Potsdam Institute for Climate Impact Research, Potsdam, Germany
[8]Intelligent Earth UKRI AI Centre for Doctoral Training in AI for the Environment, University of Oxford, Oxford, UK
[9]Climate Resource, Melbourne, Australia
[10]Max-Planck-Institute for Meteorology, Hamburg, Germany
[11]Department of Estuarine and Delta Systems, NIOZ Royal Netherlands Institute for Sea Research, Yerseke, The Netherlands
[12]Faculty of Geosciences, Department of Physical Geography, Utrecht University, Utrecht, The Netherlands
[13]Met Office Hadley Centre, Exeter, UK
[14]School of Geography, University of Bristol, UK
[15]School of Mathematics and Statistics, Rochester Institute of Technology, USA

Correspondence to: Alexander Nauels (nauels@iiasa.ac.at) and Tessa Möller (moeller@iiasa.ac.at)

Abstract. Simplified sea level modelling approaches calibrated against reference data, also referred to as sea level emulators, can explore future sea level rise and associated uncertainties with low computational cost. Here, we introduce the Sea Level Emulator Intercomparison Project (SLEIP) to assess available sea level emulators and identify future research needs. The SLEIP protocol has a multi-century focus with 2300 as the end year to explore more of the impact-relevant time horizon and also investigate sea level responses under temperature overshoot. SLEIP covers a total of 13 sea level datasets from the participating emulators BRICK, FACTS (7 individual emulator workflows), FRISIA, MAGICC, MP25, ProFSea and SURFER. The sea level components of participating emulators range from statistical models fitted to projections or observational data to physical parametrizations, to coarse spatio-temporal physical models. They also differ in whether and, if yes, how they account for low-confidence ice-sheet processes. To remove the influence of different climate forcings on the sea level responses, we run the participating emulators with both their native climate forcings and a common forcing from the MAGICC climate model. We provide an analysis of the emulator output for the 2300 projection horizon as well as the historical period. SLEIP fills a gap in the IPCC AR6 sea level assessment by providing 2300 projections for three additional policy-relevant pathways. In the MAGICC-forced configuration, the 2300 probability boxes (p-boxes: mean of medians, lowest 17th to highest 83rd percentile) for total global mean sea level rise relative to 1995-2014 are 0.93 m (0.30-3.15 m)

https://doi.org/10.5194/egusphere-2026-3874
Preprint. Discussion started: 2 September 2026

under the 1.5°C-consistent SSP1-1.9, 1.36 m (0.56-10.85 m) under the strong overshoot scenario SSP5-3.4-OS, and 2.08 m (0.97-11.00 m) under SSP2-4.5, which has been used as a proxy for current climate policies. Native-forced projections generally agree closely with the MAGICC-forced results, indicating that structural differences between sea level models dominate over climate forcing, with the Antarctic ice sheet as the largest source of uncertainty. The relative consistency of thermal expansion and glacier contributions largely reflects shared parametrizations and common calibration datasets rather than independent agreement. Under SSP5-3.4-OS, an overshoot sea level rise penalty of roughly 0.1 to 0.3 m persists by 2300 compared to SSP1-2.6, even after global mean surface air temperature has returned to the SSP1-2.6 level by 2150. This first phase of SLEIP provides a lay of the land of current sea level emulation. Future phases will build on this with ScenarioMIP-CMIP7 scenarios, targeted sensitivity experiments, and a potential extension toward regionally resolved projections.

1 Introduction

Sea level rise (SLR) is one of the clearest and best documented consequences of global warming. While global sea levels remained almost stable in the Holocene, the SLR has accelerated markedly since instrumental records began. Global mean sea level rose at 1.85 (1.44 to 2.26) mm yr^{-1} over 1901-2025, increased to 3.40 (3.26 to 3.54) mm yr^{-1} during the satellite era since 1993, and to 3.84 (3.01 to 4.67) mm yr^{-1} since 2018 (Forster et al., 2026). This observed acceleration represents only the early response of a system that operates on timescales much slower than atmospheric warming. As most committed sea level rise has yet to be realized and the response to warming is nonlinear with deep uncertainty around individual underlying physical processes, projections on multi-century timescales are both scientifically challenging and societally urgent (Nauels et al., 2025).

Sea level emulators - simplified and efficient models using sea level component-wise parametrizations calibrated against process-based projections, observations or both and forced by simple or reduced complexity climate models - emerge as an important tool to address this challenge. They complement computationally expensive physical models that are essential for the understanding of the sea level system but are too costly to systematically explore uncertainties in large ensembles, including across large sets of different greenhouse gas forcing scenarios. The systematic mapping of the sea level response to greenhouse gas pathways is particularly relevant for decision making at the science-policy interface, including through coupling to Integrated Assessment Models (Ramme et al., 2025).

The Sixth Assessment Report of the Intergovernmental Panel on Climate Change (IPCC AR6) made systematic use of sea level emulators to produce probabilistic projections of sea level change, with projections extending beyond the 21st century to 2300 for two selected scenarios and warming levels (Fox-Kemper et al., 2021). Emulators used in IPCC AR6, which were assembled in the Framework for Assessing Changes To Sea-level (FACTS), however differ substantially in their capacity to project longer term SLR beyond, with some methods being incapable of projecting beyond their 2100 training horizon (Kopp et al., 2023).

https://doi.org/10.5194/egusphere-2026-3874
Preprint. Discussion started: 2 September 2026

Several other sea level emulator frameworks have been developed before and since AR6, each making distinct choices about which processes to represent, how to parameterise them, and how to calibrate against process-based models or observations. Despite these advances, no systematic intercomparison of sea level emulators has been carried out to date. This stands in contrast to the broader field of climate emulation such as the established Reduced Complexity Model Intercomparison Project (RCMIP), where structured intercomparison frameworks (Nicholls et al., 2021, 2020; Romero-Prieto et al., 2025) now play a central role in clarifying the strengths, limitations, and underlying assumptions of individual approaches, and have made important contributions to IPCC AR6.

Here, we introduce the Sea Level Emulator Intercomparison Project (SLEIP), a systematic intercomparison of seven sea level emulators designed to assess similarities and divergences in their sea level projections and the underlying components and identify future research needs. Beyond quantifying projection spreads, SLEIP aims to increase the transparency of the assumptions underlying each participating emulator, and to bring to the fore structural similarities and differences between frameworks. We focus, in particular, on the performance post 2100, which is central for sea level commitment and on emulator behaviour under temperature overshoot. This paper represents the first phase of SLEIP. Its primary aim is to document the participating emulators and their responses, show how structurally diverse their approaches are, and point to key sources of inter-model spread. Future SLEIP phases will build on this with more targeted analyses.

2 Experimental design and emulator protocol

The SLEIP experimental design is illustrated schematically in Fig. 1. All participating emulators provide projections out to 2300, while individual emulator setups may only allow for projections out to 2100. Also, because simulation start years differ across models, all projections are provided relative to the IPCC AR6 1995–2014 baseline period.

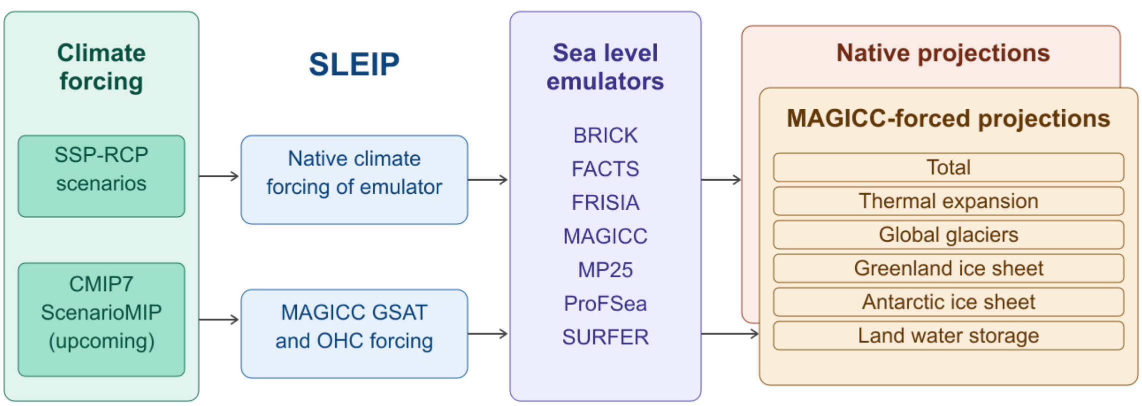

Figure 1. Schematic overview of the SLEIP experimental design, climate forcing scenarios (SSP-RCP scenarios; CMIP7 scenarios upcoming, green) are used to produce global surface air temperature and ocean heat content inputs (blue) for the participating set of sea

https://doi.org/10.5194/egusphere-2026-3874
Preprint. Discussion started: 2 September 2026

level emulators (violet). The primary MAGICC-based SLR projections (dark yellow) use the MAGICC climate forcing for all emulators. The complementary native SLR projections (red) retain each emulator's internal climate forcing.

Most participating sea level emulators are coupled to a simple climate model that translates greenhouse gas emissions into the temperature and ocean heat content changes driving the sea level response. Because these climate models differ across emulators, differences in projected sea level rise in a native multi-model comparison mix climate forcing uncertainty with structural uncertainty in the sea level models themselves. In this paper, we focus on structural differences between sea level models, and we therefore base the primary results on the simulations with identical climate forcing from MAGICCv7.5.3 (Meinshausen et al., 2020), providing global surface air temperature (GSAT) and ocean heat content (OHC) to all sea level models (Figure 2).

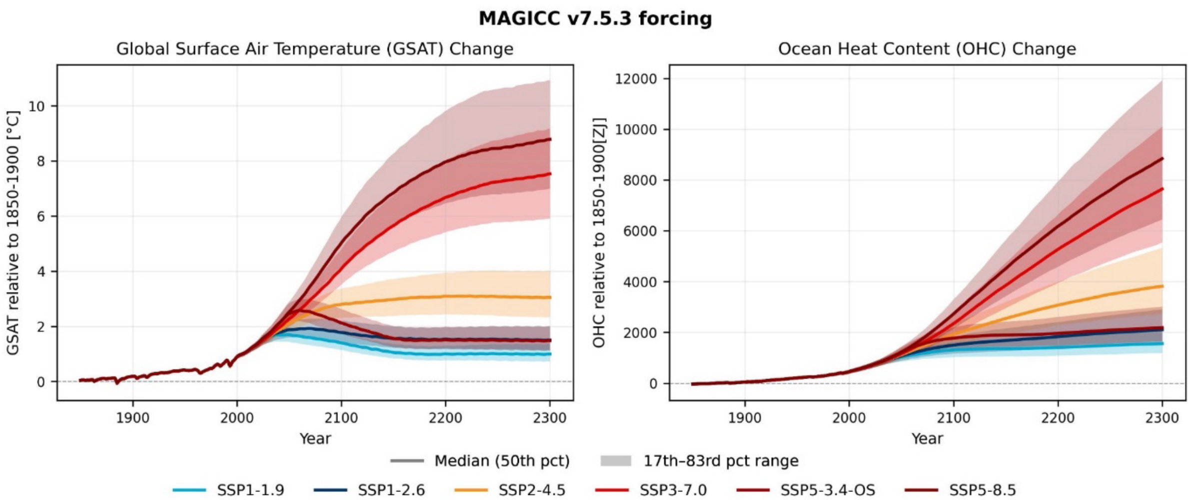

Figure 2. MAGICCv7.5.3 global surface air temperature (GSAT) and ocean heat content (OHC) changes across the six SSP-RCP scenarios SSP1-1.9, SSP1-2.6, SSP2-4.5, SSP5-3.4-OS, SSP3-7.0, and SSP5-8.5. Median (50th percentile, solid lines) and 17th–83rd percentile range (shaded bands) of MAGICC ensemble projections for (a) GSAT change relative to 1850–1900 and (b) OHC change relative to 1850–1900.

As a complementary set, emulators are also run in their native configurations with their own climate models, allowing the additional spread from the different climate models to be quantified. Both sets of simulations cover six SSP-RCP scenarios and their extensions out to 2300: SSP1-1.9, SSP1-2.6, SSP2-4.5, SSP5-3.4-OS, SSP3-7.0, and SSP5-8.5 (Riahi et al., 2017; Meinshausen et al., 2020). The requested Global Mean Sea Level Rise (GMSLR) output variables are listed in Table 1.

Table 1. Requested SLEIP output variables.

Variable Name	Description
Sea Level Change | Total	Total Global Mean Sea Level Rise (GMSLR)
Sea Level Change | Thermal Expansion	GMSLR from thermal expansion
Sea Level Change | Global Glaciers	GMSLR from glaciers mass loss

https://doi.org/10.5194/egusphere-2026-3874
Preprint. Discussion started: 2 September 2026

Sea Level Change | Greenland	GMSLR from Greenland ice sheet mass loss
Sea Level Change | Antarctica	GMSLR from Antarctic ice sheet mass loss
Sea Level Change | Land Water Storage	GMSLR from land water storage changes

2.1 MAGICC-forced projections

In the primary SLEIP configuration, all participating emulators are driven by the same MAGICC climate forcing. The reduced-complexity carbon cycle-climate model MAGICCv7.5.3, the IPCC AR6-consistent version of MAGICC (Meinshausen et al., 2020, 2011b, a), is used to translate climate forcings into global mean surface air temperature (GSAT) and ocean heat content (OHC) change. MAGICC represents the Earth system using two hemispheric atmospheric boxes, coupled to a two-box hemispherically resolved upwelling-diffusion-entrainment ocean with 40 vertical layers, and provides projections of atmospheric greenhouse gas concentrations, effective radiative forcing, surface temperature change, and Earth system heat uptake, amongst others. Probabilistic climate projections for the SSP-RCPs are generated using a 600-member ensemble, with parameter distributions constrained to reproduce observed historical warming and consistent with the assessed climate uncertainty ranges of the IPCC AR6. The resulting GSAT and OHC trajectories for the six SLEIP SSP-RCP scenarios are shown in Fig. 2. Each emulator receives the full 600-member ensemble of GSAT and OHC trajectories as input, replacing its native climate model where one exists.

2.2 Native climate model projections

In the complementary native configuration, each emulator is run with its own internal climate model. The individual native climate model settings are described alongside the respective sea level emulators in Section 3. MP25 does not contribute to this configuration as it has no integrated climate model. Comparing the estimates of this native configuration against the MAGICC-forced configuration helps to separate the climate model and SLR model influence on the SLR projections. It should be noted here that a tension can emerge when switching from native to MAGICC climate forcing because each emulator was calibrated in its native configuration under one set of forcing assumptions. Depending on the methods used for the native model calibration, this tension can lead to biases in the sea level response when running in the MAGICC-forced setup (Wong, 2026), for example, if a "high" set of calibrated emulator parameters (i.e., a set that generated a high GMSLR) were paired with a "low" set of MAGICC parameters.

3. Participating sea level emulators

Seven sea level emulators participate in this first phase of SLEIP: BRICK, FACTS, FRISIA, MAGICC, MP25, ProFSea, and SURFER. Table 2 summarises the participating sea level emulators and their key properties. In total, the SLEIP emulators contributed 13 datasets in the MAGICC-forced configuration. In this configuration, each dataset is based on the 600-member MAGICC ensemble timeseries for GSAT and OHC (Section 2.1). FACTS contributes 7 datasets (one per available emulator

https://doi.org/10.5194/egusphere-2026-3874
Preprint. Discussion started: 2 September 2026

workflow), and BRICK, FRISIA, MAGICC, MP25, ProFSea, and SURFER contribute one dataset in each configuration. The native configuration consists of 12 datasets as MP25 is not directly coupled to a climate model.

Despite sharing the same set of target sea level components, the participating emulators differ in how each component is parameterized. We classify the type of parametrization for each component: (1) empirical parameterisations, in which the functional form is a statistical fit or direct sampling from observations or model output, (2) physical parameterisations, in which the functional form is derived from physical reasoning, such as expansion proportional to ocean heat uptake, temperature-driven mass balance, or volume-area scaling; and (3) physical models, in which the component is governed by coupled ordinary or partial differential equations implementing physical laws - such as ice dynamics or multi-layer ocean dynamics. All parametrization types can be spatially resolved with regional reference data. Sea level contributions derived from structured expert judgement (SEJ) are indicated separately. In addition, Table 2 documents with two additional columns the capability of emulators to produce regional sea level rise information and the capability to handle vertical land motion to produce relative sea level estimates.

Table 2. Classification of sea level component parametrizations across participating emulators. Type 1: empirical (functional form is a statistical fit or direct sampling from observations or model output). Type 2: physical parametrization (functional form derived from physical reasoning). Type 3: physical model (coupled ODEs or multi-layer equations implementing physical laws). SEJ: structured expert judgement. The two right-most columns show spatial capabilities independent of the parametrization type: Regional output indicates whether the emulator can produce regionally resolved information; RSL indicates whether it represents vertical land motion to yield relative rather than geocentric sea level. Dash indicates components not included in an emulator. FACTS workflows are shown as a single row with differing Greenland and Antarctic ice sheet parametrization types. * MP25 uses GSAT rather than OHC as direct input for thermal expansion.

Emulator	Thermal expansion	Global glaciers	Greenland Ice Sheet	Antarctic Ice Sheet	Land water storage	Regional output	RSL functionality
BRICK	2	2	2	3	-	+	-
FACTS	2	1	1, SEJ	1, 2, SEJ	1	+	+
FRISIA	2	2	2	3	1	+	-
MAGICC	3	2	2	2	1	-	-
MP25	2*	2	2	2	1	+	+
ProFSea	2	1	1	1	1	+	+
SURFER	3	2	3	3	-	-	-

Several patterns emerge from Table 2. Thermal expansion is consistently parameterised as proportional to ocean heat content across most emulators (type 2), with MAGICC and SURFER as exceptions that resolve multi-layer ocean physics explicitly (type 3). Glacier contributions are broadly type 2 (physical mass-balance parametrizations), with ProFSea and some FACTS workflows using statistical fits calibrated to multi-model glacier output (type 1). Greenland Ice Sheet (GIS) contributions are predominantly type 2 across emulators, with SURFER's ordinary differential equation (ODE) based tipping-element

https://doi.org/10.5194/egusphere-2026-3874
Preprint. Discussion started: 2 September 2026

representation standing out (type 3), and the FACTS emulandice and FittedISMIP approaches as type 1. Antarctic Ice Sheet (AIS) contributions show the largest diversity: BRICK, FRISIA, and SURFER implement physical ice sheet models (type 3); MAGICC and MP25 use global parameterizations (type 2); ProFSea uses statistical fits to model output (type 1); and FACTS spans types 1 and 2 across its workflows, plus structured expert judgement (SEJ). Land water storage is tier 1 throughout - emulators draw from historical observations and IPCC AR6 projections, or scale contributions to population trajectories, the latter reflecting that this component's future evolution is primarily governed by socio-economic rather than physical uncertainty. Independent from the parametrization type, BRICK, FACTS, FRISIA, MP25 and ProFSea can provide regional sea level information and FACTS, MP25 and ProFSea additionally capture vertical land motion processes to produce relative sea level (RSL). As part of the first SLEIP phase presented here, only global sea level emulator output is analysed.

3.1 BRICK

The Building Blocks for Relevant Ice and Climate Knowledge (BRICK) model is a modular, semi-empirical model for sea-level change (Wong et al., 2017a). The current version is coded in Julia (v1.10), compliant with the Mimi integrated modelling framework (Anthoff and others, 2025), to facilitate coupled modelling experiments (Wong et al., 2026, 2022a). BRICK's modular structure and native coupling to a Bayesian physical-statistical modelling framework is intended to lend itself to interrogating and characterizing uncertainties stemming from physical models (both structural and parametric), statistical models, and data. BRICK is preferentially calibrated using only historical data products, as opposed to emulation of projections from process-based models. This is intended to minimize reproduction of biases from full-scale Earth system models and provide a line of evidence for future sea levels that is less dependent on these larger process models. Importantly, this design choice is not a value judgment about the benefits of model emulation versus model-data fusion (the latter being the focus of BRICK), but rather an example of model structural (including statistical model structural) uncertainty that underlies sea-level projections. This structural uncertainty is harmonious with the SLEIP goal of characterizing structural similarities and differences among different sea level modelling frameworks, and the sensitivities of sea-level projections on those structural variations. BRICK is run with separate climate forcing frameworks SNEASY and DOECLIM (Wong et al., 2022a), with SNEASY-BRICK being the native dataset analysed as part of the SLEIP ensemble, and the DOECLIM-calibrated dataset contributing to the MAGICC-forced dataset.

The thermal expansion component of BRICK computes the sea level change due to thermal expansion as proportional to the ocean heat uptake, which can be an input from either forcing data or a climate module coupled to BRICK (Vega-Westhoff et al., 2019). Two free calibration parameters characterize uncertainty in this relationship. The thermal expansion component is calibrated using trends from the IPCC AR6 (Fox-Kemper et al., 2021) and by constraining ocean heat uptake and overall GMSLR (Gouretski and Koltermann, 2004; Church and White, 2011).

The global glaciers component of BRICK is based on the model of Wigley and Raper (2005). The glacier contribution to GMSLR is computed as proportional to the product of the temperature anomaly from a hypothetical equilibrium temperature

https://doi.org/10.5194/egusphere-2026-3874
Preprint. Discussion started: 2 September 2026

(at which there would be no glacial contribution to sea-level rise), times the fraction of glacier volume remaining raised to a power. Following Wigley and Raper (2005), we take the equilibrium temperature as equal to -0.15 °C (relative to pre-industrial global mean temperature). BRICK's glacier component has six uncertain parameters, including the proportionality constant, initial glacier volume, and exponent in the power law relationship, as well as two statistical parameters within the first-order autoregressive (AR1) error model used for model-data fusion. Calibration data for the glacier component come from Dyurgerov and Meier (2005).

The GIS component of BRICK is based on the mechanistically motivated Simple Ice-sheet Model for Projecting Large Ensembles (SIMPLE) model of Bakker et al. (2016). SIMPLE computes the GIS contribution to GMSLR as proportional to the difference between the current melt-susceptible Greenland ice sheet volume and a hypothetical equilibrium ice sheet volume. The proportionality constant and equilibrium ice sheet volume are both assumed to be linearly related to global mean surface temperature anomaly, where these relationships are governed by two uncertain model parameters each. SIMPLE contains a total of five physical model parameters and two statistical parameters related to our use of an AR1 error model for calibration. Calibration data for the Greenland component come from the sea-level reconstruction of Frederikse et al. (2020).

The AIS component of BRICK is based on the Danish Center for Earth System Science Antarctic Ice Sheet (DAIS) model (Shaffer, 2014). DAIS is a two-dimensional Antarctic ice sheet model that assumes axial symmetry and represents the ice sheet mass balance from precipitation, runoff, ice flow, and ice sheet disintegration and mass loss from rising and warming sea levels. The BRICK implementation of DAIS couples to input forcing or climate modules by assuming a linear relationship between global mean surface temperature and Antarctic mean surface temperature reduced to sea level. Importantly, BRICK incorporates a pre-calibration step to assimilate 240,000 years of paleoclimate Antarctic sea level data to constrain the calibration priors for the DAIS parameters. This step is critical for constraining the large number of free parameters in DAIS (14 physical model parameters and two statistical parameters) as well as calibrating the model to represent potentially sizable Antarctic contributions to global sea level over the next few centuries (Wong et al., 2017b). The BRICK implementation of DAIS includes a stylized representation of Antarctic "fast dynamical" contributions to sea-level rise once a (uncertain) temperature threshold is exceeded. This accelerated melting mechanism is meant to represent hypothesized Marine Ice Cliff Instability (MICI) and Marine Ice Sheet Instability (MISI) as well as other potentially rapid and irreversible mass loss processes (Bassis et al., 2024; Pattyn et al., 2018; Seroussi et al., 2020). Calibration experiments indicate strong agreement between posterior inference for BRICK's uncertain AIS threshold temperature and an analogous parameter incorporated into the MAGICC sea level module (Nauels et al., 2017). However, the projections including these processes are still categorized under the IPCC AR6 low-confidence set of projections, owing to the deep uncertainty surrounding the relevant ice sheet processes.

The land water storage component of BRICK is based on mass balance trends between 2003-2013 from Dieng et al. (2015). This component assumes that the mean and variance of the distribution of land water storage annual sea level trends remains stationary throughout the span of the sea-level projections.

https://doi.org/10.5194/egusphere-2026-3874
Preprint. Discussion started: 2 September 2026

BRICK can additionally resolve regional sea level via sea level fingerprints, but without vertical land motion (i.e. geocentric, not relative). This capability is not analysed in the first phase of SLEIP.

3.2 FACTS

The Framework for Assessing Changes To Sea-level (FACTS) v1.1 (Reedy and Kopp, 2023, Kopp et al., 2023) is a modular, open-source platform designed to generate probabilistic projections of global mean sea-level (GMSL), relative sea level (RSL), and extreme sea level (ESL) change. A distinguishing feature of FACTS is its explicit design for characterizing both parametric and structural (deep) uncertainty through the parallel execution of multiple modelling workflows. FACTS is built upon the RADICAL-Cybertools computing stack, enabling scalable execution across desktop to high-performance computing environments. Development versions of FACTS modules underlie the IPCC Sixth Assessment Report (AR6) sea-level projections and the 2022 US Government sea-level rise technical report.

A FACTS experiment proceeds through four sequential steps: a climate step, a sea-level components step, an integration step, and an extreme sea-level step. In its native setting, the climate forcing step is provided by the FaIR v1.6.4 climate model emulator using AR6-calibrated parameters, which translates emissions scenarios into probability distributions of global mean surface air temperature (GSAT) and ocean heat content. These outputs drive the subsequent sea-level component modules. Information exchange between steps is mediated via the file system, allowing individual steps to be bypassed by supplying precomputed inputs.

The central organizational concept is the workflow: a specified combination of sea-level component modules whose outputs are aggregated in the integration step. Multiple overlapping workflows can share common modules while substituting alternatives for specific components, enabling systematic comparison across modelling approaches. In this analysis, seven workflows are included, closely aligned with those used in IPCC AR6. In the context of this paper, a single workflow can be thought of as a distinct sea-level emulator, assembled from different modular building blocks.

Sterodynamic sea level is derived by sampling time-invariant thermal expansion coefficients from the CMIP6 ensemble and multiplying by emulated ocean heat content. GIS contributions are represented by two alternative modules: emulandice/GrIS (FACTS workflows 1e, 2e, 3e), a Gaussian process emulator of ISMIP6 simulations from 27 modelling groups driven by GSAT; and FittedISMIP/GrIS (FACTS workflows 1f, 2f, 3f), a parametric emulator fitting projected contributions as a cubic function of GSAT and quadratic function of time, with the advantage of providing rate estimates.

AIS contributions are provided by four alternative modules representing the primary source of structural uncertainty: emulandice/AIS (FACTS workflow 1e), a Gaussian process emulation of ISMIP6; ipccar5/AIS (FACT workflow 1f), an implementation of the Antarctic Ice Sheet projection method used in the IPCC AR5 (Church et al., 2013); larmip/AIS (FACTS workflows 2e, 3f), a linear response functions from 16 ice sheet models under basal melt forcing, via LARMIP-2 (Levermann et al., 2020); deconto21/AIS (FACTS workflows 3e, 3f), a direct sampling from (DeConto et al., 2021), incorporating marine ice cliff instability; and bamber19/icesheets (FACTS workflow 4), capturing the structured expert judgment from (Bamber et al., 2019), covering both ice sheets.

https://doi.org/10.5194/egusphere-2026-3874
Preprint. Discussion started: 2 September 2026

Global glaciers are represented by emulandice/glaciers (Gaussian process emulation of the GlacierMIP2 ensemble of 11 modeling groups, FACTS workflows 1e, 2e, 3e) and ipccar5/glaciers (recalibrated to GlacierMIP2, projecting glacier melt as a nonlinear function of integrated GSAT, FACTS workflows 1f, 2f, 3f, 4).

The land water storage sea level component relates reservoir storage and groundwater depletion to SSP-specific population projections, with a correction that only 80% of depleted groundwater reaches the ocean. Vertical land motion (VLM) and glacial isostatic adjustment are following (Kopp et al., 2014) which estimated constant long-term trends at tide gauge locations via Gaussian process spatiotemporal analysis, using a GIA model as a prior mean.

FACTSv1.1 differs from FACTSv1.0 and the development version of FACTS employed in IPCC AR6 through the incorporation of an interpolated sampling scheme for the bamber19/icesheets and deconto21/AIS modules (Reedy and Kopp, 2023), enabling projections for these modules to be produced under all scenarios, not just the scenarios employed in the papers against which they are calibrated.

Although not employed in this paper, FACTS has the capacity to produce RSL projections that incorporate the gravitational, rotational, and deformational effects of barystatic sea-level contributions, as well as regional contributions of ocean dynamic sea level, calibrated against the CMIP6 model ensemble. It can also produce extreme sea level (ESL) projections using a peak-over-threshold approach fitted to GESLA-2 tide gauge data, augmented by RSL projections to estimate changes in flood return periods.

Parametric uncertainty is sampled via Monte Carlo methods (2,000 samples per workflow in this implementation). Structural uncertainty is assessed by comparing across workflows, which in application can subsequently be combined into probability boxes (p-boxes) to summarize the range of probability distributions arising from alternative modelling choices (Kopp et al., 2023).

3.3 FRISIA

FRISIA is a model designed to study the impacts of SLR with a focus on the inclusion of global socio-economic feedback (Ramme et al., 2025). It includes an internal emulator of global mean SLR that is largely based on existing frameworks and calibrated towards observations (Horwath et al., 2021) and projections from the IPCC AR6 (Fox-Kemper et al., 2021). FRISIA reads in time series of GSAT and OHC as external input, which, in its native setup and the used FRISIA version 1.0.1, are provided by the FaIR climate emulator version 2.1.1 in calibration version 1.1.0 (Smith et al., 2018; Leach et al., 2021). Optionally, global population data can be provided to drive the land water storage component of SLR. Here, population data are taken from the IIASA SSP database (Riahi et al., 2017; Kc and Lutz, 2017). FRISIA accounts for uncertainty in all the GMSLR components by varying a set of uncertainty parameters within a calibrated range in a Monte Carlo approach.

The thermal expansion component of GMSLR is calculated as a linear function of ocean heat content changes with an expansion coefficient of 0.11 ± 0.01 m/YJ in FRISIA. The central value and range of the expansion coefficient are the result of a comparison of literature values (Church et al., 2011; Fox-Kemper et al., 2021; Levitus et al., 2012; Marti et al., 2022)

https://doi.org/10.5194/egusphere-2026-3874
Preprint. Discussion started: 2 September 2026

and the model calibration. The contribution of mountain glacier melt to SLR is calculated using a nonlinear function of the GSAT anomaly and the remaining mountain glacier volume (Wigley and Raper, 2005). The temperature sensitivity and exponent of this formulation both serve as uncertainty parameters, with ranges determined during the model calibration.

The Greenland ice sheet contribution to SLR is separated into a surface mass balance (SMB) and a solid ice discharge (SID) component, as implemented in the MAGICC model version 6 (Nauels et al., 2017). The SMB component is a quadratic function of the GSAT anomaly, and proportional to the root of the remaining fraction of the ice sheet volume. The SID component is limited to a maximum of 0.42 m (Winkelmann and Levermann, 2013) and has the GSAT anomaly in the exponent of the temperature term. A high impact, low likelihood contribution can be activated via a model switch, adding a constant additional discharge above a GSAT anomaly threshold.

The Antarctic ice sheet contribution to SLR is implemented as in the BRICK model version 0.2 (Wong et al., 2017a), which applies the Danish Center for Earth System Science Antarctic Ice Sheet (DAIS) model (Shaffer, 2014). The DAIS model takes in Antarctic surface air and ocean temperatures, which are derived from the GSAT anomaly, and tracks the volume and radius of an idealized axisymmetric ice sheet. Similar to the Greenland ice sheet contribution, a high impact, low likelihood contribution can be activated via a model switch, based on the implementation in (Wong et al., 2022b).

FRISIA provides two methods to calculate the land water storage component of SLR: If global population time series are provided, FRISIA assumes that the annual land water storage change rate is proportional to the global population size (Kopp et al., 2014; Rahmstorf et al., 2012). If no population data are available, a constant annual rate is assumed. Both methods are calibrated to reproduce historical data and IPCC AR6 projections.

Like BRICK, FRISIA can additionally provide regionally aggregated sea level information, but without resolving vertical land motion. This capability is not analysed in the first phase of SLEIP.

3.4 MAGICC-SLR

MAGICC-SLR (Nauels et al., 2017a, b, and 2025) is directly integrated into the reduced-complexity simple climate carbon cycle model MAGICC (Meinshausen et al., 2011a, b, and 2020), with MAGICCv7.5.3 as the IPCC AR6-consistent model version applied here. Total GMSLR is computed as the sum of the process-based sea level contributions: thermal expansion, global glacier melt, GIS surface mass balance (SMB) and solid ice discharge (SID) changes, AIS SMB and SID changes, as well as variations in land water storage.

The thermal expansion sea level component is computed by integrating the ocean heat content across the 40 hemispheric ocean layers in MAGICC using layer-specific thermal expansion coefficients, calibrated against CMIP5 potential ocean temperature and steric sea-level change (Lorbacher et al., 2015).

Global glaciers are parameterized as a global surface air temperature (GSAT)-sensitive mass balance function, with volume-area scaling used to track the progressive depletion of glacier mass as warming continues. The parameterization is calibrated against transient and equilibrium projections out to 2300, using CMIP5 climate forcing (Marzeion et al., 2012, 2014).

https://doi.org/10.5194/egusphere-2026-3874
Preprint. Discussion started: 2 September 2026

The parameterizations of the GIS SMB and SID components are calibrated against ISMIP6-protocol simulations (Greve and Chambers, 2022), using the SICOPOLIS ice-sheet model forced by four CMIP6 models under SSP1-2.6 and SSP5-8.5, with end-of-21st-century climate conditions held constant through the year 3000. In MAGICC-SLR, Greenland SMB is represented as a polynomial function of global mean temperature anomaly, updated to include a threshold temperature at which the SMB would switch from a negative to a positive GMSLR contributor, in line with published estimates (Noël et al., 2021). Greenland SID is parameterized as a two-term function capturing the initial temperature-sensitive acceleration of outlet glacier discharge and its subsequent exponential decline as glacier retreat reduces ocean contact, a self-limiting process with a maximum cumulative contribution capped at the maximum SID contribution found in the reference dataset. Parameters are optimized through 2500. The full update of the Greenland components is described in Nauels et al. (2025). For SLEIP, the total Greenland response is reported as the sum of MAGICC-SLR SMB and SID projections.

The AIS contribution combines separately calibrated SMB and SID parameterizations. The SMB component has been calibrated against Golledge et al. (2019) based on the PISM ice-sheet model forced under RCP4.5 and RCP8.5. The SID component is calibrated against Edwards et al. (2019), who revisited the DeConto and Pollard (2016) projections by constraining the ensemble to members consistent with historical changes, using an ice-sheet model emulator. The MAGICC-SLR AIS SID component is calibrated against reference data up to the year 2300 under RCP2.6, RCP4.5, and RCP8.5 scenarios (DeConto and Pollard, 2016; Edwards et al., 2019). Only no-MICI ensemble members are used, capturing rapid ice discharge without invoking MICI. The AIS SID signal is isolated by subtracting the SMB contribution from the total AIS response. The full update is described in Nauels et al. (2025). For SLEIP, the total Antarctic response is reported as the sum of MAGICC-SLR SMB and SID projections.

Land water storage is implemented as a climate-independent contribution, prescribed from two observational and modelling datasets (Frederikse et al., 2020; Turner et al., 2023). Historical changes over 1900–2018 are taken from Frederikse et al. (2020), with future projections through 2300 following Turner et al. (2023), who link dam impoundment and groundwater extraction to population dynamics, consistent with the IPCC AR6 methodology. We adopt the SSP2 (medium population growth) trajectory throughout, applied uniformly across all climate scenarios. Continuity between the two datasets is ensured by extending the Turner et al. (2023) projections backwards to 2019 based on the 2020–2030 decadal trend.

3.5 MP25

MP25 (Perrette and Mengel, 2025) builds on a Bayesian spatial model to generate probabilistic projections of relative sea level rise and its components at 578 tide gauge locations, driven by an externally provided global mean temperature pathway. Although MP25 was designed primarily for local relative sea level projections at tide gauge sites, its global sea level components are directly applicable to the SLEIP protocol. Unlike several of the other participating emulators, MP25 does not include an integrated climate model and takes global mean temperature as direct input. Global sea level change is computed as the sum of contributions from mountain glaciers in 19 regions, the GIS and AIS contributions, thermal

https://doi.org/10.5194/egusphere-2026-3874
Preprint. Discussion started: 2 September 2026

expansion and land water storage. Sea level fingerprints translate each global contribution to local sea level change at each tide gauge site. For SLEIP, only the GMSLR components are used.

Glacier mass loss is parameterised as a temperature-sensitive function with volume-area scaling to account for progressive glacier depletion, calibrated against observational reconstructions (Frederikse et al., 2020; Malles and Marzeion, 2021; Zemp et al., 2019) and IPCC AR6 medium confidence projections for 2100 under SSP5-8.5 (Fox-Kemper et al., 2021). Ice sheet contributions are modelled with a quadratic dependence on global mean temperature, constrained jointly by historical reconstructions (Frederikse et al., 2020) and IPCC AR6 medium confidence projections for 2100 under SSP1-2.6 and SSP5-8.5 (Fox-Kemper et al., 2021). Thermal expansion is parameterised as a linear function of global mean temperature, with regional fingerprints derived from CMIP6 simulations, and constrained by historical reconstructions (Frederikse et al., 2020) and IPCC AR6 medium confidence projections for 2100 under SSP1-2.6 and SSP5-8.5 (Fox-Kemper et al., 2021). Land water storage is sampled directly from historical reconstructions and IPCC AR6 projections.

Model parameters are estimated within a Bayesian framework, with the posterior constrained by local observations: tide gauge records from 578 stations, GPS-derived vertical land motion (2000-2020), and satellite altimetry trends (1993–2019). MP25 originally provides projections to 2100 only. For SLEIP, an extension to 2300 is produced without a recalibration of the model as a pure extrapolation exercise.

3.6 ProFSea

The Met Office's Projecting Future Sea Level (ProFSea) tool v3.0 (Weeks et al., 2023) computes process-based, spatially resolved estimates of GMSL change. In this version, a 1,000,000-member Monte Carlo ensemble of GMSLR estimates are computed by the summation of individual sea level components. Thermal expansion is computed by taking the OHC directly from FaIR and MAGICC and multiplying by the mean and standard deviation of the AR6 expansion coefficients (0.113 ± 0.013 m/YJ) following (Turner et al., 2023). The Land Water Storage component is directly taken from the AR6 projections under SSP3-7.0 for all scenarios due to minimal scenario dependence.

Global glacier sea level contribution is parameterized using the AR5 formulation for glacier mass loss (Church et al., 2013) as described in (Palmer et al., 2020), but recalibrated to emulate GlacierMIP2 simulations (Marzeion et al., 2020).

The GIS response to warming is modelled following Fox-Kemper et al. (2021) and Kopp et al. (2023), with the corresponding FACTS implementation. The parameterization emulates the response of the 21-model ensemble involved in the ISMIP6 21st century GIS projections experiments (Goelzer et al., 2020).

AIS projections are calculated using parameterizations of the West Antarctic Ice Sheet, East Antarctic Ice Sheet and Antarctic Peninsula and their response to global warming - calibrated to a subset of the ISMIP6 23rd century Antarctic Ice Sheet projections (Seroussi et al., 2024). ISMIP6 experiments which include ice shelf collapse forcing are not included during calibration, and the total AIS contribution is just the sum of these regional projections.

ProFSea has the capability to provide relative sea level projections for global coastlines. This capability is not analysed in the first phase of SLEIP.

https://doi.org/10.5194/egusphere-2026-3874
Preprint. Discussion started: 2 September 2026

3.7 SURFER

SURFER v3.0 (Couplet et al., 2025) is a simple Earth system model implemented as 17 coupled ODEs, simulating global mean temperature, sea level rise, and ocean acidification in response to CO_2 and CH_4 emissions. It extends SURFER v2.0 (Martínez Montero et al., 2022) by incorporating dynamic alkalinity cycling, $CaCO_3$ sediments, and weathering fluxes, enabling simulations across timescales from decades to millions of years. The atmosphere is in thermal equilibrium with the surface ocean layer, and temperature anomalies in the three layers evolve through a heat exchange parameterization yielding a transient climate response of 1.9 °C. Radiative forcing includes CO_2, CH_4, and optionally stratospheric aerosol injection.

GMSLR is computed as the sum of four contributions: thermosteric expansion, mountain glaciers, the GIS and AIS, with a combined sea level potential of approximately 62.9 m. Thermosteric rise is the product of layer-specific thermal expansion coefficients and temperature anomalies across the three ocean layers. The coefficients are derived from GLODAPv2.2016b climatologies (Lauvset et al., 2016). Because SURFER does not represent land temperatures, all radiative imbalance is absorbed by the ocean, leading to some overestimation of thermosteric rise on centennial timescales; on millennial timescales, simulated thermosteric rise agrees well with the UVic2.8 Earth system model of intermediate complexity (Weaver et al., 2001). Mountain glacier melt relaxes toward an equilibrium as a function of surface temperature anomaly, with a sea level potential of 0.5 m, a temperature sensitivity of 2 °C, and a relaxation timescale of 200 years. The Greenland and Antarctic ice sheets are represented as tipping elements via a cubic ordinary differential equation for the volume fraction of each ice sheet relative to its preindustrial volume. The polynomial on the right-hand side encodes a bifurcation structure with two stable equilibria (a large ice sheet and a small or absent one) separated by an unstable equilibrium. The bifurcation points are calibrated to the steady-state behaviour of more complex ice sheet models, set at $T^+ = 1.52$ °C and $T^- = 0.3$ °C for Greenland (sea level potential 7.4 m), and $T^+ = 6.8$ °C and $T^- = 4.0$ °C for Antarctica (sea level potential 55 m). Melting and refreezing operate on strongly asymmetric timescales: for Greenland, $\tau^- = 470$ yr (melting) and $\tau^+ = 5500$ yr (refreezing); for Antarctica, $\tau^- = 3000$ yr and $\tau^+ = 5500$ yr. A smooth transition between these timescales replaces the discontinuous step used in SURFER v2.0, preventing spurious timescale switching near equilibrium.

A key feature of this formulation is the ability to simulate tipping point overshoot: an ice sheet can cross its critical warming threshold without irreversibly collapsing if the duration of the exceedance is short relative to the effective melting timescale. Under intermediate-emission scenarios (SSP2-4.5 and SSP4-6.0), peak warming in SURFER v3.0 exceeds the Greenland tipping threshold of 1.52 °C, yet the GIS avoids collapse because temperatures subsequently decline on millennial timescales due to long-term carbon cycle drawdown. This distinction reduces projected long-term GIS contributions by up to ~6 m under intermediate scenarios. This behaviour is absent in SURFER v2.0, where CO_2 stabilizes at elevated levels once ocean invasion is complete. For Antarctica, which has a much higher tipping threshold, collapse does not occur under any tested scenario, but the lower committed temperatures in SURFER v3.0 still reduce the long-term AIS contribution by ~8 m under SSP3-7.0 and ~18 m under SSP5-8.5 compared to SURFER v2.0.

https://doi.org/10.5194/egusphere-2026-3874
Preprint. Discussion started: 2 September 2026

4. SLEIP sea level projections

4.1 Sea level rise by 2100 and 2300

We assess the spread in sea level rise projections between emulators at two key time horizons, the years 2100 and 2300, and for both the MAGICC-forced and the native model configuration. Figures 3 and 4 show the projected sea level rise resolved by component across all SLEIP runs at 2100 and 2300 for both configurations and under all six scenarios. Provided relative to 1995-2014, total MAGICC-forced projections at 2100 are broadly consistent with IPCC AR6, with model medians clustering around approximately 0.35 m under SSP1-1.9 and around 0.85 m under SSP5-8.5. The spread between model medians is moderate at 2100 but widens substantially towards 2300, where median projections under SSP5-8.5 span from around 2 m to around 10 m depending on the emulator run. The differences in medians are driven largely by differences in Antarctic ice sheet projections, with differences in the upper tail of 2300 projections dominated by differences in ice sheet sensitivity assumptions (see Section 4.3).

Comparing MAGICC-forced with native climate model runs, we find that the choice of climate forcing hardly matters for most models and components: MAGICC-forced and native projections are often closely together, with similar spreads throughout both time horizons. This indicates that the two climate forcing setups are relatively similar and that structural differences between sea level models dominate the inter-model range regardless of the forcing choice. Two exceptions stand out. First, thermal expansion, where MAGICC-forced variants cluster more tightly across models which is an expected consequence of all emulators receiving the same OHC trajectory. But even here, the within-model shift from switching forcing is modest. Second, the BRICK native climate variant (SNEASY) produces Antarctic ice sheet projections that differ markedly from its MAGICC-forced run, which is however calibrated to a different climate model (DOECLIM). The difference is most visible under low emission scenarios at 2100.

FACTS stands out in both figures as it contributes seven bars for the total SLR panel, one for each of its emulator workflows. Because all seven workflows share identical sterodynamic and land water storage modules, the corresponding component panels show only one set of bars. For glaciers, the seven workflows are split into two groups - workflows 1e, 2e, and 3e (using emulandice) and workflows 1f, 2f, 3f, and 4 (using a parametric IPCCAR5/GlacierMIP2 representation) - which produce two distinct glacier responses for each scenario and time horizon. For Greenland, there are three distinct responses as emulandice is used by workflow 1e, 2e, and 3e, the FittedISMIP approach by 1f, 2f, and 3f; and structured expert judgement alone for workflow 4. The Antarctic ice sheet panels show the largest spread among FACTS workflows, with four distinct groups: emulandice (1e and 1f), LARMIP-2 (2e and 2f), the DeConto et al. (2021) model including marine ice-cliff instability (3e and 3f), and structured expert judgement (workflow 4).

https://doi.org/10.5194/egusphere-2026-3874
Preprint. Discussion started: 2 September 2026

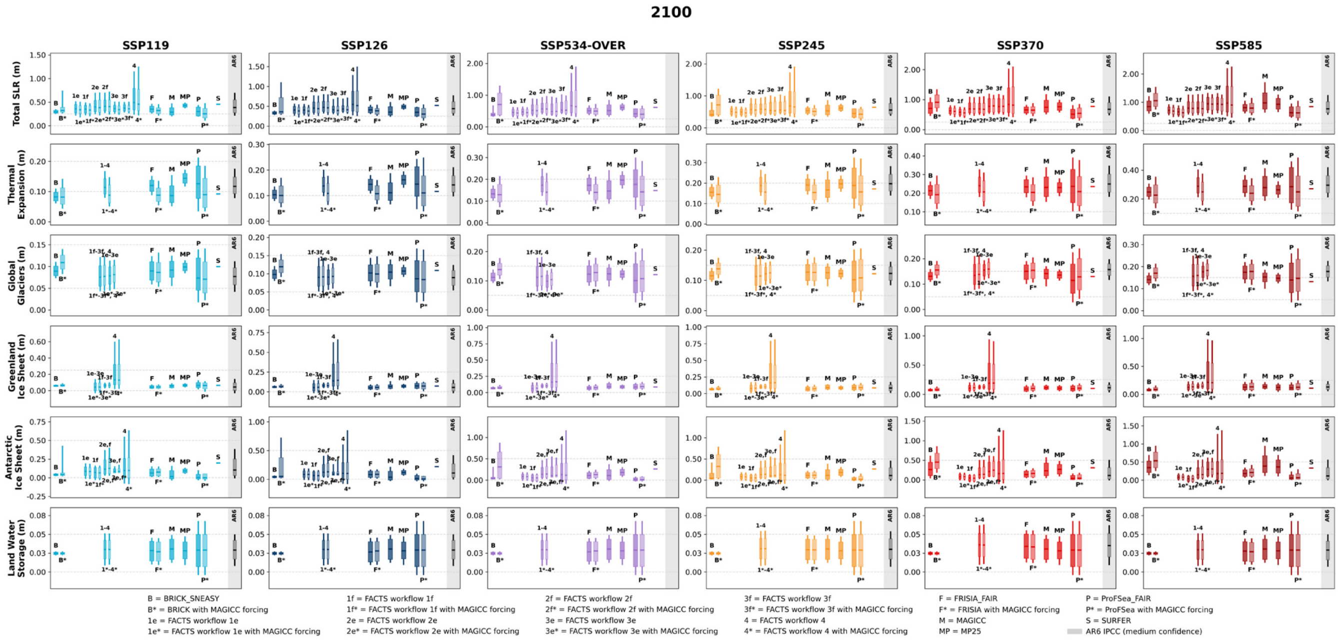

Figure 3. Sea level rise projections for year 2100 per component and across SSP-RCP scenarios for native and MAGICC-forced SLEIP runs. Boxplots show the projected sea level equivalent (SLE, relative to 1995–2014 [m]) in 2100 for each emulator, with boxes spanning the 17th–83rd percentile range, whiskers extending to the 5th and 95th percentiles, and the horizontal line indicating the median (50th percentile). Abbreviations denote the model as indicated in the legend; an asterisk (*) indicates MAGICC-forced estimates. IPCC WGI AR6 projections are included on the right side of each panel if assessed.

https://doi.org/10.5194/egusphere-2026-3874
Preprint. Discussion started: 2 September 2026

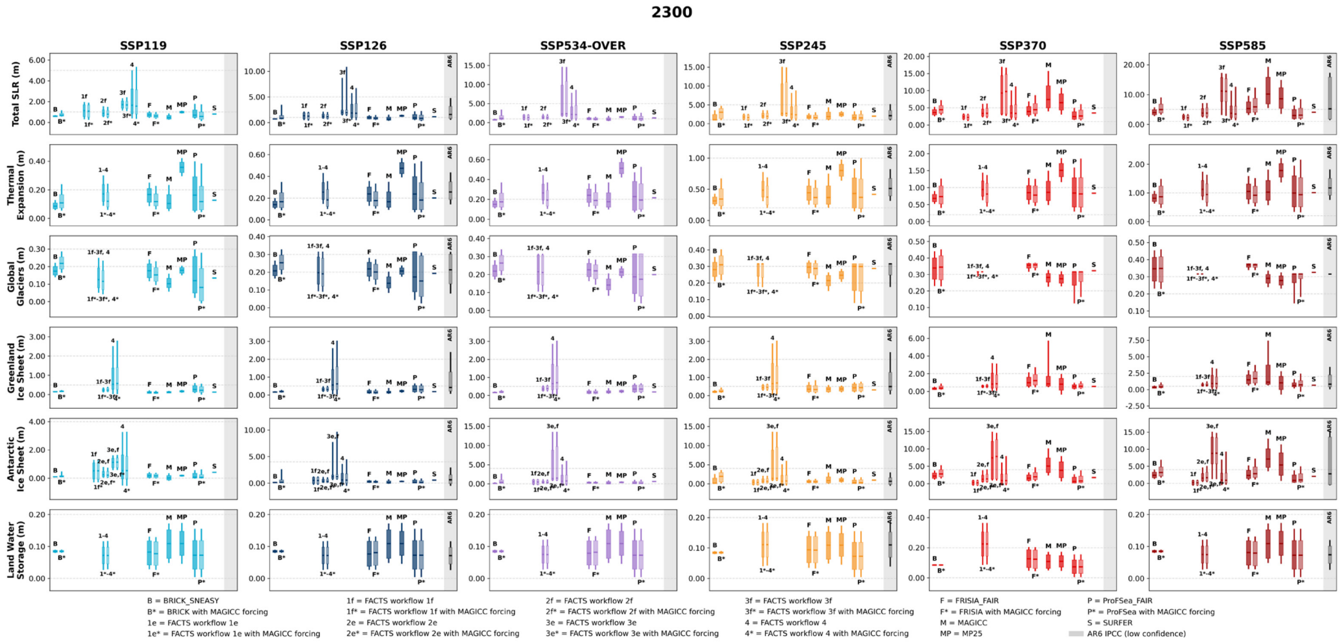

Figure 4. Sea level rise projections for year 2300 per component and across SSP-RCP scenarios for native and MAGICC-forced SLEIP runs. Boxplots show the projected sea level equivalent (SLE, relative to 1995–2014 [m]) in 2300 for each emulator, with boxes spanning the 17th–83rd percentile range, whiskers extending to the 5th and 95th percentiles, and the horizontal line indicating the median (50th percentile). Abbreviations denote the model as indicated in the legend; an asterisk (*) indicates MAGICC-forced estimates. IPCC WGI AR6 projections are included on the right side of each panel if assessed.

https://doi.org/10.5194/egusphere-2026-3874
Preprint. Discussion started: 2 September 2026

4.2 Sea level contributions over time

Thermal expansion and global glacier sea level components show relatively consistent responses across models, which largely reflects the similarity of their parametrizations and training data rather than agreement across independent approaches. Thermal expansion scales with scenario (higher warming, higher contribution) and is tightly clustered among MAGICC-forced runs, with model medians ranging from around 0.1 m under SSP1-1.9 to 0.3 m under SSP5-8.5 at 2100, and from around 0.1 m to 1.1 m, respectively, by 2300. Glacier contributions are limited by their total available volume and their decreasing sensitivity with decreasing volume. This shows in both figures with similar responses in 2100 and a strong convergence by 2300 as a near-complete depletion of global glacier volume is approached under moderate to high forcing. Most models plateau at around 0.3 m sea level equivalent (SLE) from glaciers under high scenarios, overall consistent with the estimated total global glacier volume outside the ice sheets of approximately 0.32 m SLE (Farinotti et al., 2019), with BRICK and FRISIA as an exception, which are calibrated against Wigley and Raper (2005) that assumed a maximum glacier SLE contribution of 0.41 m. Land water storage shows negligible inter-emulator spread throughout, as parametrizations largely draw from the same underlying IPCC AR6 datasets.

The AIS contributes most of the SLR projection uncertainty in agreement with the current science (Fox-Kemper et al., 2021; Seroussi et al., 2024). Already in 2100, the AIS is the largest single GMSLR source for most emulators, with medians ranging from close to zero to above 0.5 m under SSP5-8.5 - a range that often exceeds the sum of all other contributions. The Antarctic contribution also drives the upper tail of the total distribution in 2100 across all scenarios, with the one exception being FACTS workflow 4, where the expert-elicitation-based Greenland ice sheet (GIS) contributes a similar magnitude. Structural differences in the parameterisation of the AIS contribution, in particular, whether and how marine ice-sheet instability processes are represented, drive the majority of total inter-model spread. The GIS shows a more structured pattern of inter-model disagreement. In 2100, the FACTS expert-elicitation-based workflow 4 stands out as an outlier across all scenarios, projecting substantially higher contributions than the process-based and parametric approaches. In 2300, the expert-elicitation results remain separated from the others under lower emissions scenarios. Under the highest scenarios, however, parametric and process-based approaches increasingly diverge among themselves, with some projecting GIS contributions comparable to or exceeding the expert-elicitation estimate, reflecting the growing sensitivity of these approaches to sustained high forcing over multi-century timescales.

Figure 5 shows absolute component contributions for four 30-year time periods, three scenarios, and all emulator runs. Relative contributions are provided in a corresponding figure in the Supplementary Information. Under SSP1-1.9 and SSP5-3.4-OS, the FACTS LARMIP-2 workflows (2e and 2f) produce net negative Antarctic contributions. These two workflows combine the LARMIP-2 dynamic ice discharge with an Antarctic SMB term taken from the IPCC AR5 parameterisation (Church et al., 2013), reducing sea level following the approximation the SMB accumulation increases at 5.1 ± 1.5% per degree Celsius of Antarctic warming.

https://doi.org/10.5194/egusphere-2026-3874
Preprint. Discussion started: 2 September 2026

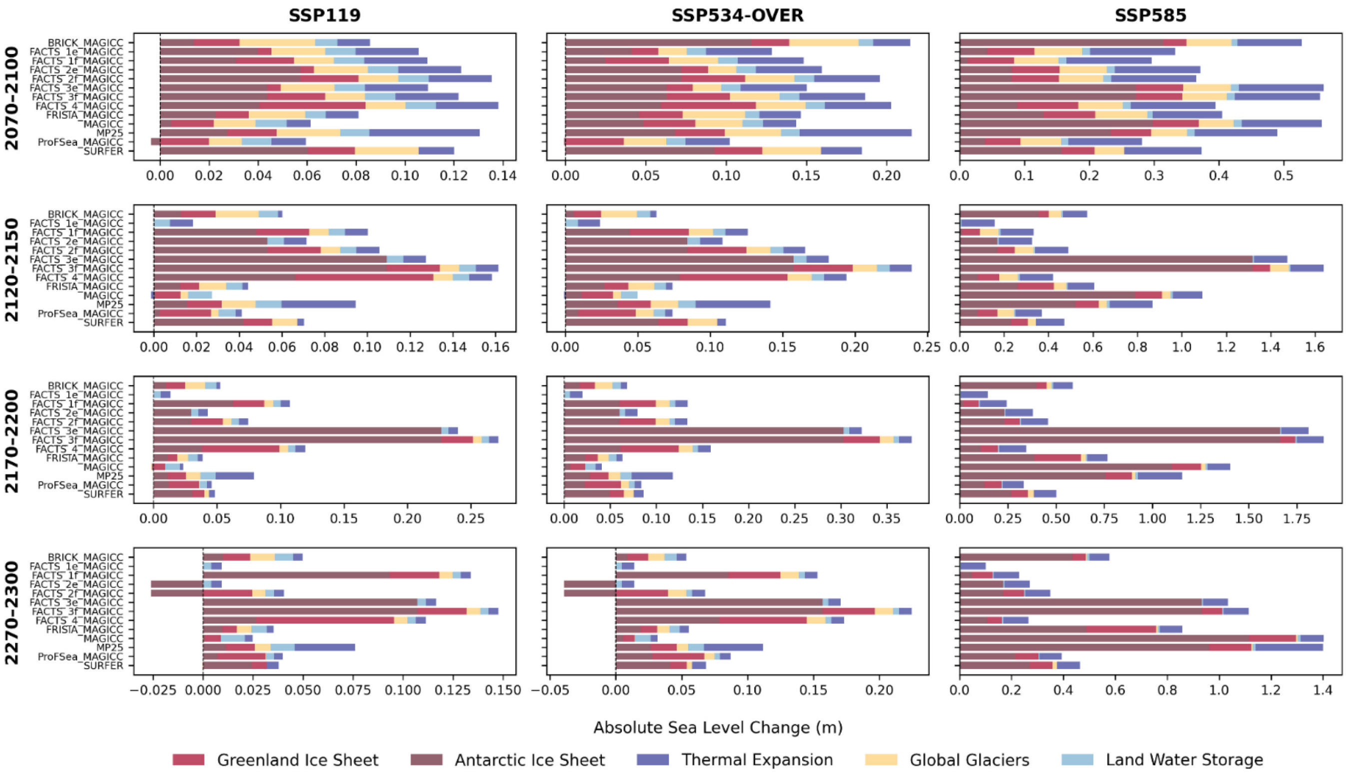

Figure 5. Absolute component contributions to global mean sea-level rise per emulator for selected scenarios and time periods. Stacked bars show the median absolute contribution of each sea level component to the median total GMSLR in meters per emulator and time period. Panel rows correspond to four 30-year time periods (2070-2100, 2120-2150, 2170-2200, 2270-2300), columns to three selected scenarios (SSP1-1.9, SSP5-3.4-OS, SSP5-8.5). Negative contributions (bars extending left of zero) indicate components where the modelled response reduces total sea level rise in the respective period.

Under low forcing, this SMB gain appears to exceed the small LARMIP-2 dynamic discharge response, yielding a net negative Antarctic contribution. MAGICC-SLR's multi-layer ocean model produces slightly negative thermosteric contributions in later time periods under the strong overshoot scenario SSP5-3.4-OS due to the persistent negative forcing resulting in a pronounced warming reversal. Simpler emulators do not capture this reversal. Under SSP5-8.5, Antarctic ice discharge increasingly dominates for later time periods (except for FACTS workflow 1e), while the role of glaciers diminishes as glacier volumes approach complete depletion. Under SSP1-1.9 and SSP5-3.4-OS, the picture is more heterogeneous, with the AIS contribution still dominating for many but not all emulators.

4.3 Sea level sensitivity to climate forcing

Sea level components respond to climate forcing in a slow, delayed, and integrative way rather than an instantaneous one. This behaviour was formalized in previous work as the transient sea level sensitivity (TSLS), defined as the change in the rate of sea level rise per unit change in global mean surface temperature (Grinsted and Christensen, 2021). Grinsted et al.

https://doi.org/10.5194/egusphere-2026-3874
Preprint. Discussion started: 2 September 2026

(2022) showed that most contributors to sea level rise have a near time-invariant TSLS, with glaciers and ice caps as an exception as they have comparatively shorter response time and shrinking area as melt progresses. Separately, Hermans et al. (2021) showed that global mean sea-level change in 2100 is more accurately predicted by the time-integral of GSAT change up to that point than by the instantaneous GSAT value in 2100, since the relationship between GMSL and GSAT itself becomes less linear toward 2100, while the relationship with time-integrated GSAT remains close to linear and largely scenario-independent. These findings motivate our assessment of sea level responses versus time-integrated, cumulative GSAT in this section. Because all MAGICC-forced emulators in this analysis receive the identical GSAT trajectory, their cumulative GSAT response is the same for each emulator at a certain time step. Any spread between emulator lines at a given cumulative GSAT value therefore reflects structural differences between sea level models without any contribution from climate forcing differences.

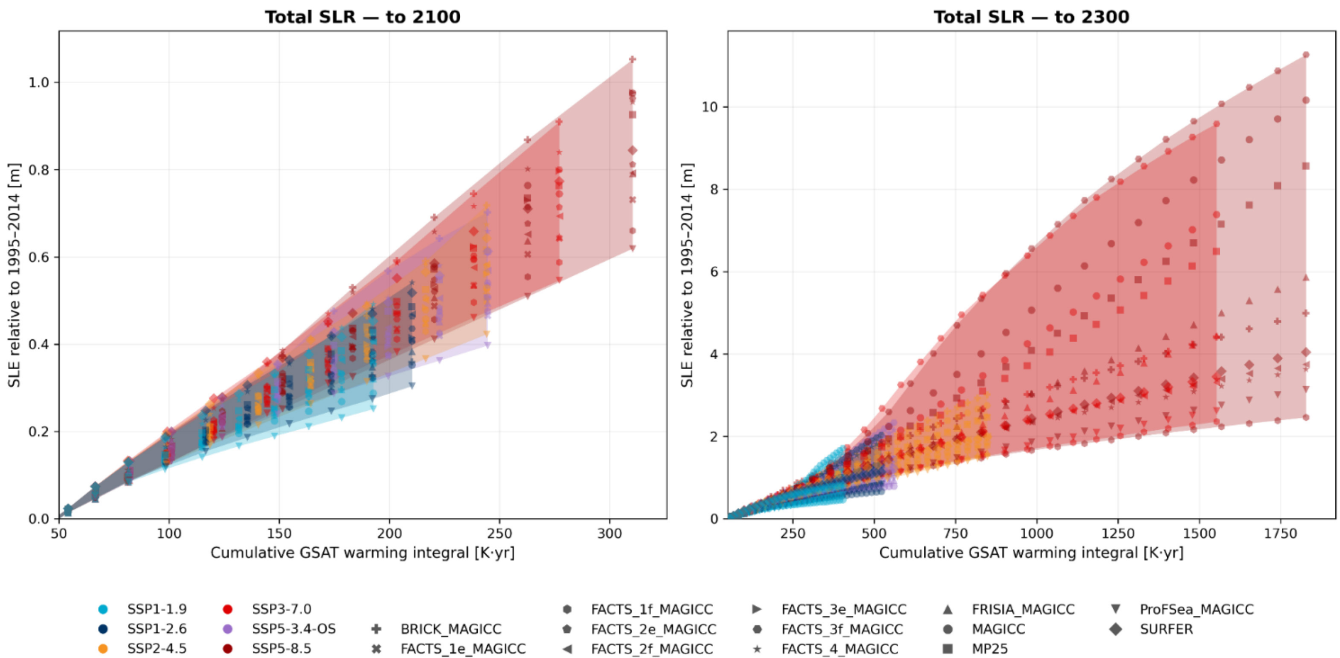

Figure 6. Cumulative GSAT warming integral versus total sea level response for SLEIP runs across all scenarios out to 2100 and 2300. Cumulative MAGICC GSAT warming integral (∫ GMT dt from 1850 up to the year 2100 and 2300 for of each data point, [K·yr]) against sea level equivalent (SLE, relative to 1995–2014) for the total SLR responses across SSP1-1.9, SSP1-2.6, SSP5-3.4-OS, SSP2-4.5, SSP3-7.0, and SSP5-8.5 scenarios. Each line represents the 50th percentile emulator response, with colours denoting the scenario and symbols denoting individual models as indicated in the legend. Shaded areas indicate the 50th percentile response range across emulators per scenario.

How each emulator correlates climate change to sea level change for 2100- and 2300-time horizons is shown in Fig. 6, with median total sea level response per emulator plotted against the cumulative GSAT warming integral from 1850 under all SSP-RCP scenarios. For the 21st century, a quasi-linear relationship between cumulative GSAT and the total sea level rise

https://doi.org/10.5194/egusphere-2026-3874
Preprint. Discussion started: 2 September 2026

responses of the emulators can be identified, while also a small scenario specific signal emerges. For the 2300-time horizon, linearity is weakened at least for several emulator responses, in particular the ones which emulate high-impact, low-likelihood process-based projections including MICI (DeConto et al., 2021).

To assess how each emulator correlates climate change to sea level change across its individual components, we plot in Fig. 7 the median sea level response per component of each emulator against the cumulative GSAT warming integral from 1850 (please see Supplementary Information for more detailed figures per emulator). Consistent with Sections 4.1 and 4.2, thermal expansion responses are tightly clustered across emulators, increasing sub-linearly with cumulative GSAT, basically reflecting the MAGICC ocean heat content response. This matches the modest structural disagreement reported for steric sensitivity in CMIP6 (Grinsted et al., 2022). MP25 is an exception, parameterising thermal expansion as directly proportional to the cumulative GSAT integral and thus the only emulator with a linear relationship by construction. Volume depletion is visible for the glacier contributions in the integral GSAT space, with rapid initial growth and then flattening for higher cumulative forcing. BRICK and FRISIA show glacier contribution beyond the ~0.32 m, consistent with their higher depletable glacier volume (see Section 4.2). Even though SSP5-8.5 reaches extreme warming, the spread of the glacier contribution at the end of the simulations is still on the order of 10 cm with saturation often not fully reached.

GIS contributions show a broadly linear scaling with cumulative GSAT across emulators. It is notable that a similar response emerges despite substantial structural diversity in how the GIS component is implemented (Table 2). This near-linear behaviour agrees with Grinsted et al. (2022), who state that the modelled GIS response is likely driven mainly by surface mass balance rather than ice dynamics, especially for higher temperatures. FACTS workflow 4 projects substantially higher GIS at equivalent cumulative forcing than the other emulators except for SSP5-8.5, consistent with the outlier behaviour already noted for the years 2100 and 2300 in Section 4.2. The convexity (accelerating response at higher cumulative warming) suggests that experts encode a higher and nonlinear sensitivity of the Greenland ice sheet to sustained warming. This may be due to expert consideration of threshold behaviour or poorly constrained high-end dynamics that is not well captured by the emulator parametrizations (or their training data).

The AIS is the most structurally diverse component across the SLEIP ensemble, with emulators differing not only in the magnitude of their projected contributions but also in the functional form of their response. Even under the lowest forcing scenario (SSP1-1.9), the spread in form and magnitude is already substantial, which shows high structural uncertainty independent of the forcing magnitude. Under sustained high warming (SSP5-8.5), the divergence between emulators is extreme: AIS contributions range from less than 0.5 m to more than 8 m.

The range exceeds the ones from all other components together, showing the central role of Antarctica for longer-term sea level projections. Emulators that include MICI (FACTS workflows 3e and 3f) show strongly accelerating ice loss, leading to the highest estimated contribution for 3 of the 4 scenarios. A further qualitatively distinct behaviour appears in FACTS workflows 2e and 2f (LARMIP-2): under SSP1-1.9 and the overshoot scenario SSP5-3.4-OS, their AIS contribution reverses after peak warming, declining as the cumulative integral continues to grow.

https://doi.org/10.5194/egusphere-2026-3874
Preprint. Discussion started: 2 September 2026

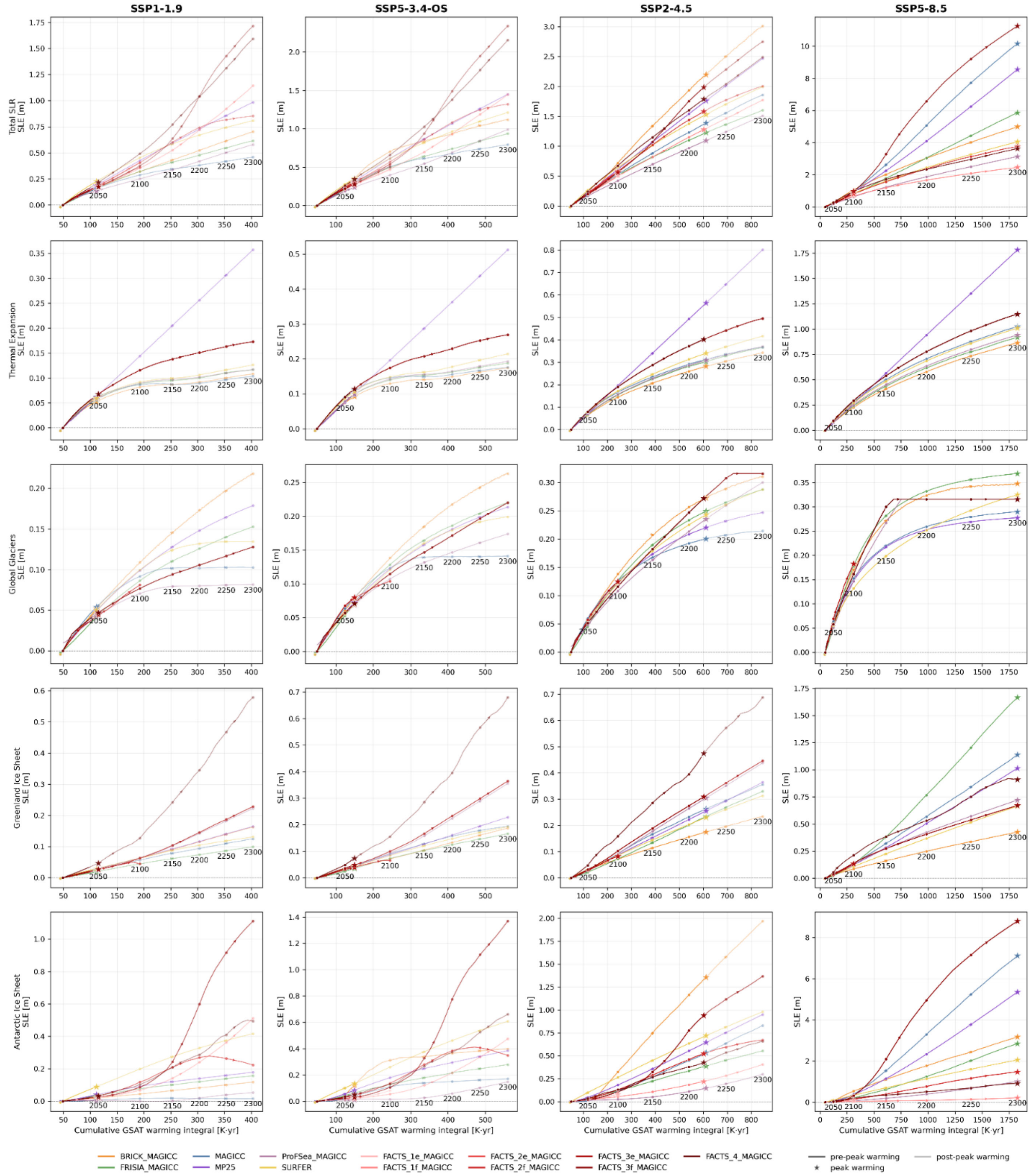

Figure 7. Cumulative GSAT warming integral versus component-wise sea level contributions for SLEIP runs across selected scenarios. Cumulative MAGICC GSAT warming integral (∫ GMT dt from 1850 up to the year 2300 for of each data point, [K·yr]) against sea level equivalent (SLE, relative to 1995–2014) for climate-forcing sensitive SLR components across SSP1-1.9, SSP5-3.4-OS, SSP2-4.5, and SSP5-8.5 scenarios. Each line represents the 50th percentile emulator response, with colours denoting individual models as indicated in the legend. Peak warming is indicated as a star, post-peak GSAT change is plotted with less opacity, 50-year time increments are indicated to include information on temporal evolution.

https://doi.org/10.5194/egusphere-2026-3874
Preprint. Discussion started: 2 September 2026

As discussed in section 4.2, this potentially reflects the dominance of SMB accumulation over dynamic discharge under low and declining forcing in these workflows, leading to a partial reversibility not captured by most other emulators. Most cases where a strong departure from linearity occurs are in the post-peak parts of the sea level trajectories.

The total GMSLR response largely reflects the AIS dominance in longer-term sea level rise in the emulators. The inter-model spread in total SLR grows with cumulative forcing: lines that are reasonably clustered at low cumulative GSAT diverge, with differences amplifying as warming accumulates. Under SSP1-1.9 and SSP5-3.4-OS, the spread has a bimodal character due to the MICI-containing FACTS workflows (3e and 3f) combined with the other sea level contributions. Under SSP5-8.5, there is a wide spread as emulators diverge substantially with no single model or workflow dominating the range. The total SLR response under SSP2-4.5 is more linear compared to the other scenarios. This may be due to the near-plateau character of the SSP2-4.5 temperature evolution in the 22nd and 23rd centuries. The almost constant forcing seemingly leads to convergence in the form of response for total sea level.

4.4 Sea level emulator behaviour under overshoot

Overshoot scenarios in which temperatures exceed a warming target for a limited time before returning back down to below the target pose challenges to sea level emulators. One reason is that emulators are mostly trained with scenario data that does not assume net-negative CO2 emissions to reverse the GSAT increase. Much less process-based model data is available on system behavior under temperature stabilization or decline. This limitation is especially pronounced for ice sheets, whose responses have often been evaluated under very high emissions (RCP8.5/SSP5-8.5) but less with a lower emissions scenario with net-negative CO2 emissions achieved towards the end of the 21st century (RCP2.6/SSP1-2.6) (Seroussi et al., 2020, 2024). This leaves only few data to constrain ice sheet dynamics under lower-warming stabilization or overshoot pathways. Research on how sea level components respond to a global mean temperature decrease is only in its early stages (Feenstra et al., 2025; Lacroix et al., 2024; Leloup et al., 2025; Schuster et al., 2025; Smith et al., 2026).

Nonetheless, in this section, we aim to bring to the fore the behaviour of the current sea level emulator generation under overshoot utilizing the SSP5-3.4-OS and SSP1-2.6 scenario output. We compare the emulator responses under the strong overshoot scenario SSP5-3.4-OS directly with the ones under SSP1-2.6 in Fig. 8. The two scenarios show diverging GSAT trajectories in the first half of the 21st century and their trajectories converge again around 2150 (Fig. 8 top panel). Thus, from 2150 onwards both scenarios result in (almost) the same forcing on the sea level system. Any difference in sea level contributions after 2150 is therefore attributable exclusively to the SSP5-3.4-OS temperature overshoot relative to the SSP1-2.6 response before 2150.

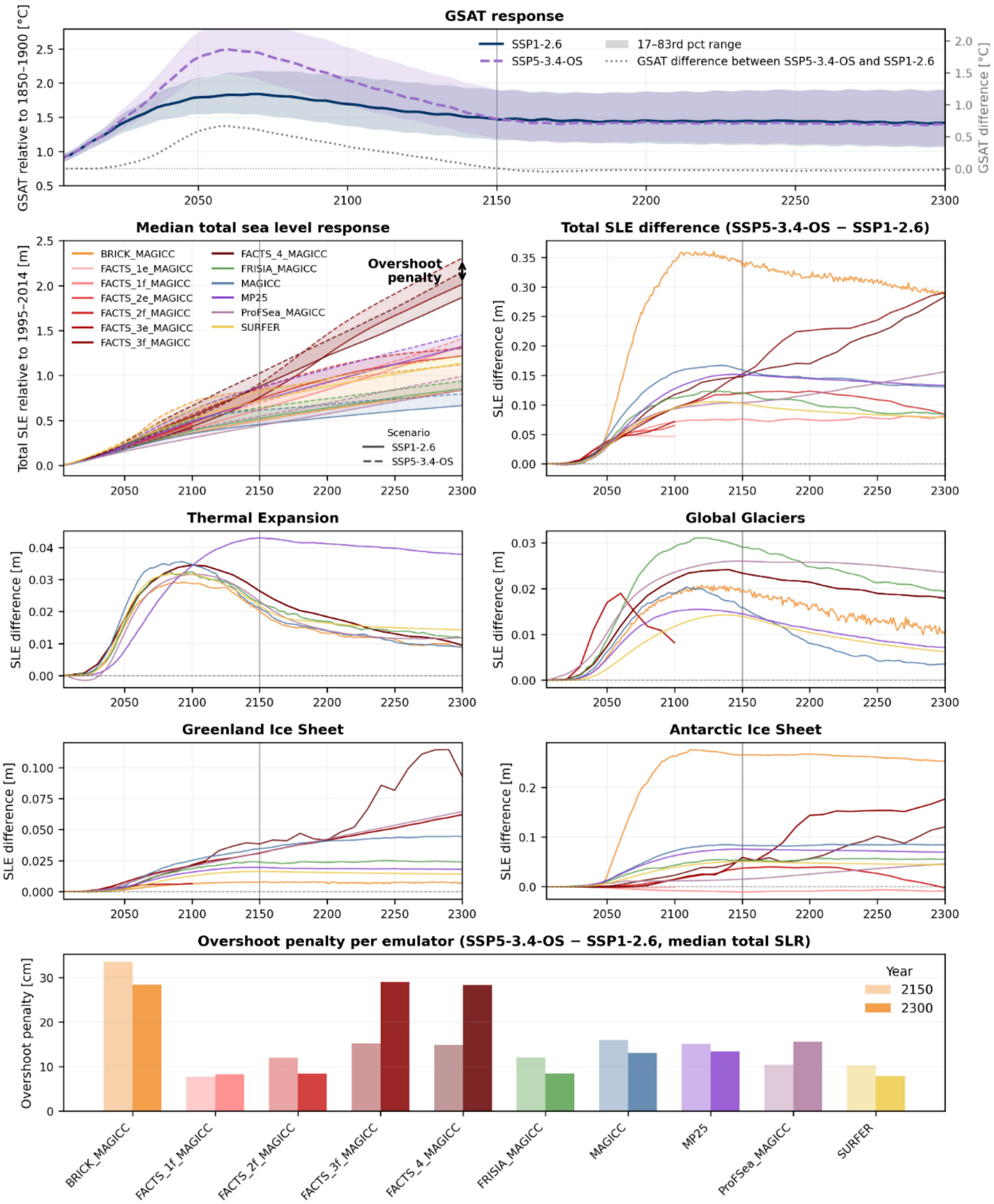

Figure 8. Emulator sea level commitment from the additional SSP5-3.4-OS temperature overshoot compared to SSP1-2.6. (A) GSAT evolution for SSP1-2.6 (solid black) and SSP5-3.4-OS (dashed violet) with 17th-83rd percentile shading across the MAGICC ensemble; the GSAT difference between the two scenarios (dotted black) is shown on the right y-axis. The vertical line marks 2150, where the two scenario GSAT trajectories reconverge. (B) Median total sea level response for all MAGICC-forced emulators under both scenarios; the overshoot penalty is the vertical gap (dashed to full line) between scenario pairs at any given time. (C-G) Time series of the SLR difference (SSP5-3.4-OS minus SSP1-2.6) per emulator for total SLR, thermal expansion, global glaciers, Greenland ice sheet, and Antarctic ice sheet. (H) Overshoot penalty per emulator at 2150 and 2300, defined as the median total SLR difference between SSP5-3.4-OS and SSP1-2.6. Colours identify individual emulators as in the legend.

https://doi.org/10.5194/egusphere-2026-3874
Preprint. Discussion started: 2 September 2026

The component panels reveal clear emulator differences across the main sea level drivers. Thermal expansion differences are small in magnitude and tightly clustered across emulators, which is due to the same MAGICC OHC forcing and the similarity in parametrizations of thermal expansion between emulators. MP25 is the exception as it computes thermal expansion from a direct GSAT scaling rather than MAGICC ocean heat content. Glacier contributions show a wider spread between emulators than thermal expansion, often with a slow partial recovery (glacier growth) after the GSAT convergence in 2150. Greenland and Antarctic contributions in contrast are largely irreversible on the timescale shown, with the overshoot penalty persisting and continuing to grow after 2150 in four emulator datasets. Again, the Antarctic ice sheet is the most diverging component between emulators: BRICK projects the largest Antarctic SLR penalty with a sharp onset in 2050. This propagates directly into the largest total SLR difference over most of the assessed time horizon, only equalled in 2300 by FACTS workflows 3f and 4 reaching a similar penalty.

We summarize the total SLR overshoot penalty at 2150 and 2300 in the bottom panel of Fig. 8. The SLR penalties in 2300 lie in the range of roughly 8 cm (FACTS_1f) to 29 cm (FACTS_3f), representing an additional 6% (FACTS_1f) to 34% (BRICK) of total 2300 GMSLR relative to the SSP1-2.6 2300 response. For six out of the ten emulators which provide 2300 projections, the penalty decreases from 2150 towards 2300, as thermal expansion and glacier contributions begin to reverse under the extended negative GSAT forcing. Four out of the ten emulators show a growing penalty through 2300, reflecting dominating ice sheet contributions with high inertia. BRICK and FACTS workflows 3f and 4 form the upper range and project a penalty of up to 30 cm by 2300.

The results shown here should be interpreted with care. We only look at one overshoot scenario pair, as SSP1-2.6 and SSP5-3.4-OS are the only scenarios with GSAT convergence in the SSP-RCP set, limiting the form and range of overshoot we could assess. Feedbacks important for multi-century projections such as the elevation-temperature feedback or the albedo-melt feedback necessarily have only simplified representations or are absent in the SLEIP emulators. We can therefore expect an underrepresentation of structural uncertainty in the overshoot responses of available SLEIP emulators. Please see the Discussion Section 6 for the broader context of emulator use for overshoot assessments.

4.5 Combined sea level projections

To summarize the presented SLR projections, we employ a probability box (p-box) framework. We estimate likely ranges for total SLR as well as for individual sea level components. The p-box framework represents uncertainty by constructing an envelope from percentile bounds across multiple models and was also used in AR6 to produce projections from multiple datasets. For SLEIP, the p-boxes include emulator responses in the range of the AR6 low confidence assessment (Fox-Kemper et al., 2021).

Throughout, the p-box bounds capture the minimum 17th and maximum 83rd percentile across emulators, and the median estimate reflecting the mean of the individual emulator medians (50th percentiles). In our implementation, projections from each emulator are always treated as independent, while the FACTS workflows are reflected differently in the total and the component p-boxes. For total SLR, all seven FACTS workflows are included as independent in the p-box aggregation. For

https://doi.org/10.5194/egusphere-2026-3874
Preprint. Discussion started: 2 September 2026

thermal expansion, FACTS workflows are grouped into one response as the component behaves the same across workflows. The same is true for the land water storage component. For the glacier component, FACTS workflows are grouped into two sets (1e–3e and 1f–3f, 4), reflecting their distinct glacier representations. For the GIS, FACTS workflows are grouped into three distinct responses (1e-3e, 1f-3f, 4), and for the AIS, five FACTS workflow groups are considered (1e, 1f, 2e-f, 3e-f, and 4). This grouping ensures that component-specific process differences are not double-counted, while it introduces a minor inconsistency for the number of total SLR p-box estimates.

We present p-box–based projections for the years 2100, 2150, and 2300 using MAGICC-forced projections (see Table 3, Table 4, and Table 5), and compare these results with the corresponding AR6 p-box estimates. In AR6, projections are separated into low- and medium-confidence categories. In contrast, we do not differentiate between these confidence levels and reflect all participating emulator components within one p-box.

A negative lower bound for the Antarctic Ice Sheet contribution is present across all scenarios and time horizons, reflecting model variants in which enhanced SMB accumulation over the Antarctic interior outweighs dynamic mass loss. In 2100, this contrasts the AR6 p-box projections, which do not show negative AIS lower bounds under any scenario. In 2300, however, SLEIP captures the AR6 assessment that indicates that negative AIS contributions under low-emission scenarios are possible.

By 2100, SLEIP central estimates are broadly consistent with AR6 across all scenarios. The SLEIP lower bound is systematically below respective AR6 medium confidence projections, mainly reflecting the negative AIS tail. Under SSP5-8.5, SLEIP median projections sit between the medians of the AR6 medium- and low-confidence estimates. The upper bound of SLEIP reflects the upper bound of the AR6 low-confidence range.

Table 3. Ensemble p-box GMSLR projections derived from MAGICC-forced SLEIP runs across six SSP-RCP scenarios for the year 2100, relative to 1995-2014. For each scenario and component, the lower bound reflects the minimum 17th percentile across models, the upper bound reflects the maximum 83rd percentile, and the central estimate represents the mean of model medians (50th percentile). All sea level equivalent contributions are provided in meters.

2100 MAGICC-forced SLEIP projections
p-box: mean p50 (min p17 - max p83); relative to 1995-2014 in meters
*low confidence projections

Component	SSP1-1.9	SSP1-2.6	SSP5-3.4-OS	SSP2-4.5	SSP3-7.0	SSP5-8.5
Thermal expansion	0.09 (0.05-0.14)	0.11 (0.06-0.18)	0.14 (0.08-0.21)	0.16 (0.09-0.24)	0.21 (0.13-0.29)	0.26 (0.15-0.36)
Global glaciers	0.09 (0.04-0.13)	0.10 (0.05-0.14)	0.12 (0.06-0.17)	0.12 (0.06-0.17)	0.15 (0.08-0.20)	0.16 (0.09-0.23)
Greenland Ice Sheet	0.07 (0.00-0.32)	0.08 (0.01-0.37)	0.09 (0.02-0.45)	0.10 (0.04-0.43)	0.12 (0.06-0.51)	0.14 (0.06-0.55)
Antarctic Ice Sheet	0.07 (-0.02-0.27)	0.07 (-0.01-0.38)	0.12 (-0.02-0.66)	0.12 (-0.02-0.60)	0.18 (-0.03-0.68)	0.22 (-0.04-0.77)

https://doi.org/10.5194/egusphere-2026-3874
Preprint. Discussion started: 2 September 2026

Land water storage	0.03 (0.01-0.05)	0.03 (0.01-0.05)	0.03 (0.01-0.05)	0.03 (0.01-0.05)	0.03 (0.01-0.05)	0.03 (0.01-0.05)
Total	0.34 (0.16-0.77)	0.40 (0.20-0.89)	0.52 (0.27-1.15)	0.54 (0.29-1.13)	0.71 (0.39-1.42)	0.82 (0.45-1.55)
IPCC AR6 Total	0.38 (0.28-0.55)	0.44 (0.32-0.62) 0.45 (0.32-0.79)*	-	0.56 (0.44-0.76)	0.68 (0.55-0.90)	0.77 (0.63-1.01) 0.88 (0.63-1.60)*

By 2150, SLEIP p-box projections are also broadly consistent with AR6. For SSP5-8.5, the SLEIP upper bound of 4.66 m is in line with the AR6 low-confidence upper bound of 4.82 m, while the SLEIP lower bound of 0.84 m falls below the corresponding AR6 lower bound, reflecting emulated negative AIS contributions. For all other scenarios, the SLEIP upper bounds similarly exceed the lower bounds of the AR6 medium-confidence p-box projections.

Table 4. Ensemble p-box GMSLR projections derived from MAGICC-forced SLEIP runs across six SSP-RCP scenarios for the year 2150, relative to 1995-2014. For each scenario and component, the lower bound reflects the minimum 17th percentile across models, the upper bound reflects the maximum 83rd percentile, and the central estimate represents the mean of model medians (50th percentile). All sea level equivalent contributions are provided in meters.

2150 MAGICC-forced SLEIP projections
p-box: mean p50 (min p17 - max p83); relative to 1995-2014 in meters
*low confidence projections

Component	**SSP1-1.9**	**SSP1-2.6**	**SSP5-3.4-OS**	**SSP2-4.5**	**SSP3-7.0**	**SSP5-8.5**
Thermal expansion	0.09 (0.05-0.17)	0.13 (0.07-0.23)	0.15 (0.08-0.26)	0.22 (0.13-0.36)	0.37 (0.22-0.54)	0.45 (0.26-0.67)
Global glaciers	0.11 (0.04-0.17)	0.13 (0.05-0.19)	0.15 (0.07-0.22)	0.18 (0.09-0.27)	0.24 (0.12-0.32)	0.27 (0.14-0.32)
Greenland Ice Sheet	0.11 (0.03-0.60)	0.13 (0.04-0.64)	0.16 (0.06-0.78)	0.18 (0.08-0.78)	0.25 (0.10-0.91)	0.30 (0.11-0.93)
Antarctic Ice Sheet	0.13 (-0.04-0.54)	0.14 (-0.03-0.65)	0.22 (-0.04-2.39)	0.30 (-0.05-2.36)	0.62 (-0.09-3.14)	0.79 (-0.12-3.60)
Land water storage	0.04 (0.02-0.08)	0.04 (0.02-0.08)	0.04 (0.02-0.08)	0.05 (0.02-0.08)	0.05 (0.02-0.09)	0.04 (0.02-0.08)
Total	0.49 (0.20-1.30)	0.59 (0.28-1.52)	0.76 (0.35-3.02)	0.96 (0.47-3.02)	1.57 (0.73-4.19)	1.89 (0.84-4.66)
IPCC AR6 Total	0.57 (0.37–0.86)	0.68 (0.46–0.99) 0.73 (0.46-1.34)*	-	0.92 (0.66–1.33)	1.19 (0.89–1.65)	1.32 (0.98–1.88) 1.98 (0.98–4.82)*

https://doi.org/10.5194/egusphere-2026-3874
Preprint. Discussion started: 2 September 2026

By 2300, this pattern still holds: under SSP5-8.5, the SLEIP upper bound of 15.79 m remains comparable to the AR6 low-confidence estimate of 16.2 m (which includes MICI), and for lower emission scenarios the SLEIP upper bounds are again above the AR6 medium-confidence lower bounds, reflecting the growing dominance of Antarctic ice sheet uncertainty at centennial timescales. For SSP1-2.6, the SLEIP median estimate of 1.17 m falls within the AR6 medium confidence process range of 0.6–1.5 m, while the SLEIP upper bound of 3.70 m substantially exceeds the upper bound of the lower confidence process range (2.1 m). The SLEIP upper bound is driven by the SEJ-based FACTS workflow 4.

Table 5. Ensemble p-box GMSLR projections derived from MAGICC-forced SLEIP runs across six SSP-RCP scenarios for the year 2300, relative to 1995-2014. For each scenario and component, the lower bound reflects the minimum 17th percentile across models, the upper bound reflects the maximum 83rd percentile, and the central estimate represents the mean of model medians (50th percentile). All sea level equivalent contributions are provided in meters.

2300 MAGICC-forced SLEIP projections
p-box: mean p50 (min p17 - max p83); relative to 1995-2014 in meters
*17th to 83rd percentile of the associated probability distributions, +including Marine Ice Cliff Instability (MICI)

Component	SSP1-1.9	SSP1-2.6	SSP5-3.4-OS	SSP2-4.5	SSP3-7.0	SSP5-8.5
Thermal expansion	0.11 (0.06-0.22)	0.17 (0.09-0.34)	0.18 (0.10-0.36)	0.36 (0.19-0.66)	0.80 (0.43-1.30)	0.94 (0.51-1.54)
Global glaciers	0.13 (0.00-0.26)	0.19 (0.06-0.30)	0.20 (0.08-0.31)	0.29 (0.15-0.36)	0.32 (0.25-0.41)	0.33 (0.26-0.42)
Greenland Ice Sheet	0.24 (0.06-1.41)	0.28 (0.08-1.57)	0.33 (0.10-1.63)	0.42 (0.18-1.62)	0.75 (0.24-1.90)	0.92 (0.27-3.71)
Antarctic Ice Sheet	0.34 (-0.13-1.55)	0.40 (-0.13-1.74)	0.50 (-0.14-9.70)	0.86 (-0.22-9.57)	2.60 (-0.40-12.66)	3.21 (-0.49-13.35)
Land water storage	0.08 (0.03-0.15)	0.08 (0.03-0.15)	0.08 (0.03-0.15)	0.09 (0.03-0.15)	0.12 (0.03-0.30)	0.08 (0.03-0.15)
Total	0.93 (0.30-3.15)	1.17 (0.47-3.70)	1.36 (0.56-10.85)	2.08 (0.97-11.00)	4.69 (1.51-14.78)	5.59 (1.53-15.79)
IPCC AR6 Total	-	0.6 to 1.5* 1.4 to 2.1*+	-	-	-	2.2 to 5.9* 9.5 to 16.2*+

Native-climate-forcing p-box projections are generally in close agreement with the MAGICC-forced results across all scenarios and time horizons, suggesting that sea level process uncertainty rather than climate modelling uncertainty mainly spans the overall projection envelope (see Table S1, Table S2, and Table S3 in the Supplementary Information).

https://doi.org/10.5194/egusphere-2026-3874
Preprint. Discussion started: 2 September 2026

5. Historical sea level change

We show the emulator performance over the historical period to provide a simple visual check how the participating emulators can reproduce the observed trajectory of global mean sea level change and its components. Figure 9 compares available emulator outputs against the observational reconstruction of Frederikse et al. (2020), which provides an estimate of global mean sea level change and its contributions. All emulators shown in Fig. 9 are run in their native-climate-forcing configuration, using each model's own internal climate forcing rather than the MAGICC input.

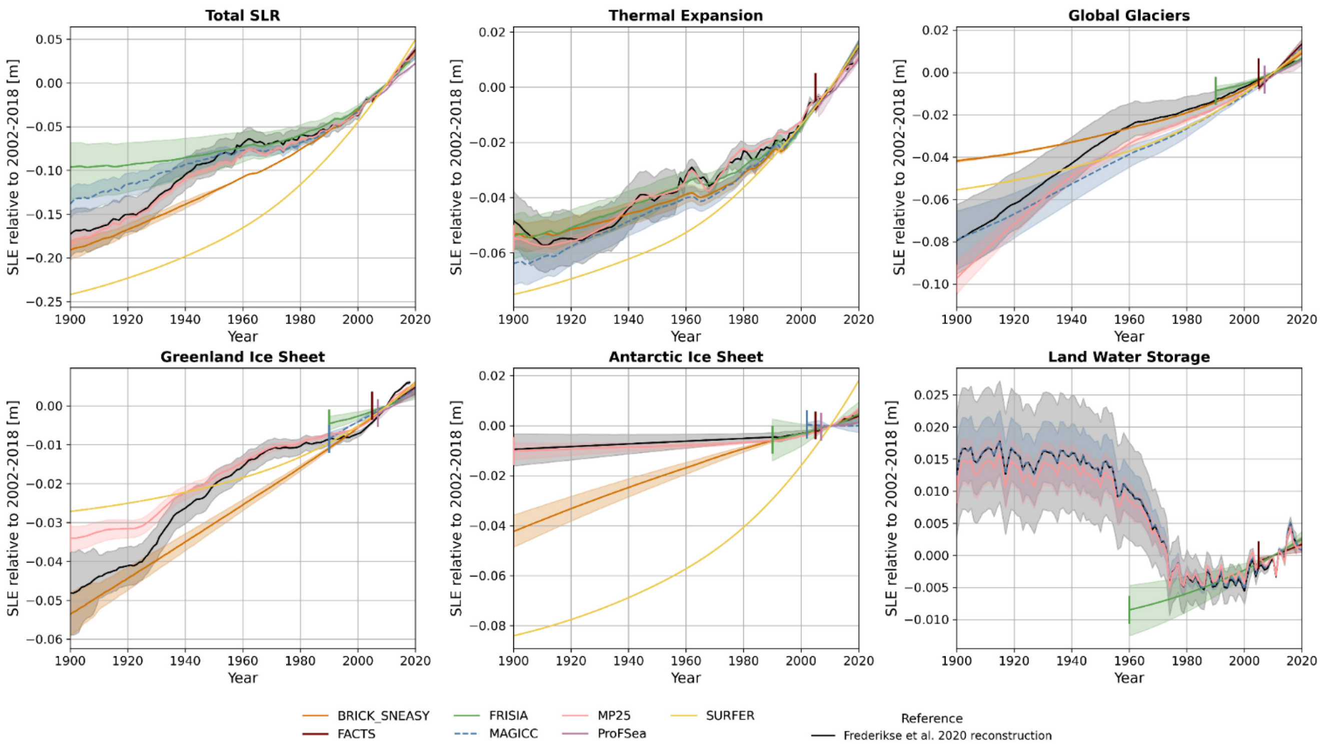

Figure 9. Historical global mean sea level change per component across participating emulators compared to the Frederikse et al. (2020) observational reconstruction. Each panel shows cumulative sea level equivalent (m, relative to 1995-2014) for total sea level rise and components. Coloured lines show the median response of each emulator's native setup for the historical time period from 1900; shaded bands indicate the 17th-83rd percentile range. A short vertical bar on each model line marks the emulator's historical start year, varying across models and components as detailed in Table TAB-START. The Frederikse et al. (2020) reconstruction is shown as a black line with grey shaded uncertainty range. BRICK and SURFER do not include a land water storage component and are absent from that panel. FACTS workflows from 2005 and ProFSea simulations from 2007 to 2014 are driven by historical forcing before scenario forcing starts.

Not all emulators provide historical simulations, and start years differ across emulators and across components within emulators as summarised in Table 6. FACTS and ProFSea are designed as pure projection frameworks and are not calibrated to reproduce historical records. Their start years fall into the end period of the CMIP6 historical simulations. The remaining five emulators - BRICK, FRISIA, MAGICC, SURFER, and MP25 - provide historical simulations to varying degrees, with start years ranging from 1750 to 2002. The actual CMIP6 SSP-RCP scenario forcing begins in 2015.

https://doi.org/10.5194/egusphere-2026-3874
Preprint. Discussion started: 2 September 2026

Total sea level rise in the historical period (Fig. 9, top left panel) is broadly reproduced across the emulators that produce multi-decadal historical records. Model medians generally follow the upward trend of the Frederikse et al. (2020) reconstruction, with most emulator ranges overlapping the observational uncertainty throughout. The degree of agreement reflects model design: MP25, which is directly calibrated against the Frederikse et al. (2020) reconstruction, is by construction close to reproducing it. MAGICC and FRISIA arrive at historical consistency less directly, through calibrated physical parameterisations driven by their own historical climate forcing. SURFER is an exception: its total sea level trajectory runs outside the observational range.

At the component level, SURFER trajectories are smoother than those of other emulators across all panels, which may be due to its focus on longer time scales through its differential equation formulations. Thermal expansion shows the tightest clustering among the emulators, which is a consequence of historically constrained OHC delivering similar inputs to similar thermal expansion parameterisations. For glaciers, the response is reasonably well captured by the emulators producing historical responses, with BRICK underestimating the contribution before 1960. For the historical contribution from Antarctica, the SURFER and BRICK contributions appear as clear outliers ranging well beyond the historical contribution of other emulators and the available observational uncertainty. As observational or modelled information on 20th century Antarctic ice mass change is very sparse, especially for the earlier part, AIS parametrizations are poorly constrained for the historical period. For the land water storage contribution, BRICK and SURFER are absent as they do not include a LWS component. MAGICC and MP25 both sample the Frederikse et al. (2020) dataset directly and therefore track it closely by construction. FRISIA stands apart, deriving land water storage from a population-based scaling rather than from observational data, and consequently shows a distinct trajectory.

Table 6. Start years of sea level component simulations for each participating emulator and average annual global mean sea level (GMSL) rate for the period 2006-2025 in mm per year. ProFSea data starts in 2007 only, hence average annual GMSL rates are provided for 2007-2026. SLEIP average annual GMSL rates are compared to the estimates of Forster et al. (2026).

	SLEIP sea level component start-years					
Emulator	**Thermal expansion**	**Global glaciers**	**Greenland Ice Sheet**	**Antarctic Ice Sheet**	**Land water storage**	**2006-2025 annual GMSL rate (central estimate, mm/yr)**
BRICK	1850	1850	1850	1850	-	3.59
FACTS	2005	2005	2005	2005	2005	3.81-4.45
FRISIA	1750	1850	1990	2002	1900	3.47
MAGICC	1750	1850	1990	2002	1900	3.41
MP25	1900	1900	1900	1900	1900	3.61
ProFSea	2007	2007	2007	2007	2007	3.09
SURFER	1850	1850	1850	1850	-	5.08
					SLEIP mean	3.82
					Forster et al. (2026)	3.67 ± 2.47

https://doi.org/10.5194/egusphere-2026-3874
Preprint. Discussion started: 2 September 2026

In order to better understand how the participating sea level emulators capture the recent past of global mean sea level (GMSL) changes, we derive the averaged annual GMSL rates of the individual emulators and the corresponding SLEIP mean for the 20-year period 2006-2025 and compare those to the estimate provided in Forster et al. (2026). With a few exceptions like SURFER (5.08 mm/yr) or FACTS workflow 4 (4.45 mm/yr), median rates of participating emulator are rather closely aligned with the central estimate of 3.67 mm/yr in Forster et al. (2026) and well within the range of observational uncertainty.

6. Discussion and outlook

Phase one of SLEIP provides the first systematic intercomparison of sea level emulators, providing an overview of the current sea level emulation landscape. The results document first insights into both the degree of agreement and the structural diversity that exist among emulators sharing the same physical target variables. Several general findings and methodological considerations emerge from this analysis.

The classification in Table 2 shows that structural diversity across emulators is uneven across components. Thermal expansion and glacier contributions are dominated by similar parameterisations and input data, and some emulators draw on the same underlying calibration datasets, particularly the Frederikse et al. (2020) reconstruction and the GlacierMIP2 and ISMIP6 data. This shared reliance on common training data reduces the effective independence of participating emulators, even where their functional forms differ. The land water storage component, while not fundamental for global SLR projections, represents a unique case in terms of how similarities between emulators relate to process understanding and uncertainty: with most emulators sampling the same observational dataset directly, the apparent agreement across models in this component reflects shared input rather than advanced process understanding narrowing the range of responses. The Antarctic ice sheet stands out as the component with the greatest structural diversity, spanning the full range from statistical fits to physical models and structured expert judgement. It drives the largest fraction of inter-model spread in both 2100 and 2300 projections. This structural diversity in AIS parameterisations reflects the large scientific uncertainty about the timing and scale of future Antarctic ice loss.

Calibration time periods and calibration data types are two axes where emulators differ. Several participating emulators were originally designed for 21st-century projections, and their extension to 2300 constitutes an extrapolation beyond the range for which they were calibrated. This is true for MP25, but also for the Greenland and glacier components of FACTS and ProFSea, which are calibrated using 21st-century ISMIP6 Greenland and GlacierMIP2 glacier simulations. Around one hundred years of calibration data is short compared to the ice sheet and deep ocean response timescales. This could lead to a response bias, which could be further investigated, for example, by comparing the multi-layer ocean behaviour of MAGICC or SURFER to simpler thermal expansion parameterisations like that of MP25. The type and time horizon of available calibration data are a key part of structural emulator uncertainty that SLEIP aims to make more transparent.

https://doi.org/10.5194/egusphere-2026-3874
Preprint. Discussion started: 2 September 2026

Sea level emulators critically depend on the quality, length and underlying climate forcing of their training data. Most of the currently available calibration datasets - including the ISMIP6 ice sheet simulations, GlacierMIP2 glacier projections, and the AR6 scenario ensemble - focus on few standard SSP-RCP pathways, with limited representation of temperature overshoot trajectories. This is a significant gap: under overshoot scenarios such as SSP5-3.4-OS, emulators are asked to project sea level responses in a world where peak warming is followed by pronounced and extended cooling. The reversibility of sea level contributions, particularly from ice sheets and the deep ocean, is highly uncertain and expected to differ between components. Robustly constraining emulator behaviour under overshoot will require dedicated long-term process-based model simulations that explicitly run overshoot trajectories, ideally spanning a large range of warming rates, peak temperatures, and cooling rates relevant to mitigation scenarios. Providing such training data should be an important priority for process-based modelling communities.

The treatment of low-confidence sea level contributions associated with the instability of the Greenland and Antarctic ice sheets varies substantially across participating emulators. This variety is a direct consequence of the deep uncertainty concerning instability, threshold behaviour and tipping, including their timing. SURFER explicitly encodes tipping point bifurcation structures for both ice sheets via its cubic differential equation formulation; FACTS includes a workflow (3e/3f) based on the DeConto et al. (2021) model incorporating marine ice cliff instability, as well as a workflow incorporating the results of a structured expert judgement elicitation of future ice-sheet changes (Bamber et al., 2019); BRICK and FRISIA use the DAIS physical ice sheet model with a stylised fast-dynamics threshold. Other emulators parametrize the Antarctic contribution without explicit tipping point representation. Consequently, the upper tail of sea level projections under high-emission scenarios is highly sensitive to which emulator - and which AIS parameterisation - is selected. Advancing the physical understanding of ice sheet dynamics on centennial timescales and translating knowledge gains into emulator parametrizations that are both physically grounded and well calibrated is one of the central challenges for the sea level emulator research community.

This paper establishes a first snapshot of the sea level emulation landscape. Several directions for future SLEIP phases are motivated by the findings presented here. First, extending the scenario set: the current SLEIP protocol covers six SSP-RCP scenarios; future phases will incorporate new ScenarioMIP-CMIP7 scenarios as they become available to be assessed by the IPCC Seventh Assessment Report. This will provide updated forcing pathways and facilitate comparisons of process-based model projections based on different scenario generations. Second, targeted sensitivity analyses - similar to the RCMIP effort (Romero-Prieto et al., 2025) - using stylised forcings such as pulse experiments, stepwise warming, constant warming rate, temperature stabilisation or idealised overshoot profiles, would allow for a more systematic assessment of sea level emulator sensitivities and calibration dependencies than what is possible with the standard SSP ensemble alone. Third, an extension of the analysis from global to regional sea level projections would substantially expand the relevance of SLEIP for impact and adaptation research, including for attribution, loss and damage assessments, and coastal planning. Frameworks like FACTS, ProFSea or MP25 already include relative sea level rise capabilities, illustrating different ways forward to fuse global with regional data.

Code and data availability

The data underlying the study can be accessed at https://doi.org/10.5281/zenodo.21027187 (Nauels et al., 2026). Supporting code to explore the data and reproduce figures and tables presented in this study can be accessed at https://zenodo.org/records/21166356. The code for the participating sea level emulators is documented and accessible through the references cited as part of the Section 3 emulator descriptions.

Author contributions

AN designed and coordinated the research, with support from TM and MM. AN, TM, VC, REK, PK, MM, GM, ZRJN, LN, and TW carried out the modelling and produced the sea level emulator data assessed in the study. AN, TM, and MM carried out the data analysis. All authors discussed the study results. AN, MM, and TM developed and wrote the manuscript, with contributions from all authors.

Competing interests

The authors declare that they have no conflict of interest.

Acknowledgements

We acknowledge the World Climate Research Programme, which coordinated the Coupled Model Intercomparison Project Phase 6 (CMIP6), including the ScenarioMIP-CMIP6 effort, which produced the SSP-RCP scenarios. We thank the climate modelling groups for producing and making available their model output used for the calibration of emulators, the Earth System Grid Federation (ESGF) for archiving the data and providing access, and the multiple funding agencies who support CMIP6 and ESGF. We would also like to acknowledge the Reduced Complexity Model Intercomparison Project (RCMIP), with its third Phase coordinated by Alexander Romero-Prieto. We also thank Matthew D. Palmer and Tamsin L. Edwards for their support, guidance and feedback.

Financial support

This research has been supported by the European Union Horizon Europe Research and Innovation programme projects FUTURA (grant-no. 101295156), SPARCCLE (grant-no. 101081369), and WorldTrans (grant-no. 101081661). REK and PK were supported by the NASA Sea Level Change Team. TM acknowledges financial support by the Luxembourgish Fond National de la Recherche (AFR PhD grant no. 18824314).

https://doi.org/10.5194/egusphere-2026-3874
Preprint. Discussion started: 2 September 2026

References

Anthoff, D. and others: Mimi: An Integrated Assessment Modeling Framework, 2025.

Bakker, A. M. R., Applegate, P. J., and Keller, K.: A simple, physically motivated model of sea-level contributions from the Greenland ice sheet in response to temperature changes, Environ. Model. Softw., 83, 27–35, https://doi.org/10.1016/j.envsoft.2016.05.003, 2016.

Bamber, J. L., Oppenheimer, M., Kopp, R. E., Aspinall, W. P., and Cooke, R. M.: Ice sheet contributions to future sea-level rise from structured expert judgment, Proc. Natl. Acad. Sci., 116, 11195 LP – 11200, https://doi.org/10.1073/pnas.1817205116, 2019.

Bassis, J. N., Crawford, A., Kachuck, S. B., Benn, D. I., Walker, C., Millstein, J., Duddu, R., Åström, J., Fricker, H. A., and Luckman, A.: Stability of Ice Shelves and Ice Cliffs in a Changing Climate, Annu. Rev. Earth Planet. Sci., 52, 221–247, https://doi.org/10.1146/annurev-earth-040522-122817, 2024.

Church, J. A. and White, N. J.: Sea-Level Rise from the Late 19th to the Early 21st Century, Surv. Geophys., 32, 585–602, 2011.

Church, J. A., White, N. J., Konikow, L. F., Domingues, C. M., Cogley, J. G., Rignot, E., Gregory, J. M., Van Den Broeke, M. R., Monaghan, A. J., and Velicogna, I.: Revisiting the Earth's sea-level and energy budgets from 1961 to 2008: Sea-Level and Energy Budgets, Geophys. Res. Lett., 38, n/a-n/a, https://doi.org/10.1029/2011GL048794, 2011.

Church, J. A., Clark, P. U., Cazenave, A., Gregory, J. M., Jevrejeva, S., Levermann, A., Merrifield, M. A., Milne, G. A., Nerem, R. S., Nunn, P. D., Payne, A. J., Pfeffer, W. T., Stammer, D., and Unnikrishnan, A. S.: Sea Level Change, in: Climate Change 2013: The Physical Science Basis. Contribution of Working Group I to the Fifth Assessment Report of the Intergovernmental Panel on Climate Change, edited by: Stocker, T. F., Qin, D., Plattner, G.-K., Tignor, M., Allen, S. K., Boschung, J., Nauels, A., Xia, Y., Bex, V., and Midgley, P. M., Cambridge University Press, Cambridge, United Kingdom and New York, NY, USA, 2013.

Couplet, V., Martínez Montero, M., and Crucifix, M.: SURFER v3.0: a fast model with ice sheet tipping points and carbon cycle feedbacks for short- and long-term climate scenarios, Geosci. Model Dev., 18, 3081–3129, https://doi.org/10.5194/gmd-18-3081-2025, 2025.

DeConto, R. M. and Pollard, D.: Contribution of Antarctica to past and future sea-level rise, Nature, 531, 591–597, https://doi.org/10.1038/nature17145, 2016.

DeConto, R. M., Pollard, D., Alley, R. B., Velicogna, I., Gasson, E., Gomez, N., Sadai, S., Condron, A., Gilford, D. M., Ashe, E. L., Kopp, R. E., Li, D., and Dutton, A.: The Paris Climate Agreement and future sea-level rise from Antarctica, Nature, 593, 83–89, https://doi.org/10.1038/s41586-021-03427-0, 2021.

Dieng, H. B., Champollion, N., Cazenave, A., Wada, Y., Schrama, E., and Meyssignac, B.: Total land water storage change over 2003–2013 estimated from a global mass budget approach, Environ. Res. Lett., 10, 124010, https://doi.org/10.1088/1748-9326/10/12/124010, 2015.

Dyurgerov, M. B. and Meier, M. F.: Glaciers and the Changing Earth System: A 2004 Snapshot, Institute of Arctic and Alpine Research, University of Colorado, Boulder, Colorado, 2005.

Edwards, T. L., Brandon, M. A., Durand, G., Edwards, N. R., Golledge, N. R., Holden, P. B., Nias, I. J., Payne, A. J., Ritz, C., and Wernecke, A.: Revisiting Antarctic ice loss due to marine ice-cliff instability, Nature, 566, 58–64, https://doi.org/10.1038/s41586-019-0901-4, 2019.

Farinotti, D., Huss, M., Fürst, J. J., Landmann, J., Machguth, H., Maussion, F., and Pandit, A.: A consensus estimate for the ice thickness distribution of all glaciers on Earth, Nat. Geosci., 12, 168–173, https://doi.org/10.1038/s41561-019-0300-3, 2019.

Feenstra, T., Vizcaino, M., Wouters, B., Petrini, M., Sellevold, R., and Thayer-Calder, K.: Role of elevation feedbacks and ice sheet–climate interactions on future Greenland ice sheet melt, The Cryosphere, 19, 2289–2314, https://doi.org/10.5194/tc-19-2289-2025, 2025.

Forster, P. M., Walsh, T., Smith, C., Lamb, W. F., Lamboll, R., Cassou, C., Hauser, M., Hausfather, Z., Lee, J.-Y., Palmer, M. D., Von Schuckmann, K., Slangen, A. B. A., Szopa, S., Trewin, B., Yun, J., P. Gillett, N., Jenkins, S., Matthews, H. D., Raghavan, K., Ribes, A., Rogelj, J., Rosen, D., Zhang, X., Allen, M., M. Andrew, R., Atkinson, C., Betts, R. A., Bombelli, A., Burgess, S. N., Cheng, L., Claxton, H. E., Friedlingstein, P., Frölicher, T. L., Domingues, C. M., Gasser, T., Gregory, C. H., Hoesly, R. M., Huppmann, D., Ishii, M., Kadow, C., Karwat, A., Kennedy, J., Killick, R. E., Kovilakam, M. V. M., Krummel, P. B., Lan, X., Lamarque, J.-F., Liné, A., Martín-Míguez, B., Monselesan, D. P., Morice, C., Mühle, J., Mussak, P., Peters, G. P., Pirani, A., Pongratz, J., Rigby, M., Rohde, R., Savita, A., Seneviratne, S. I., Smith, S. J., Taha, G., Tassone, C., Thorne, P., Wells, C., Western, L. M., Van Der Werf, G. R., Wijffels, S. E., Zecchetto, M., Zhong, J., Zhang, X., Masson-Delmotte, V., and Zhai, P.: Indicators of Global Climate Change 2025: annual update of key indicators of the state of the climate system and human influence, https://doi.org/10.5194/essd-2026-287, 23 April 2026.

Fox-Kemper, B., Hewitt, H., Xiao, C., Aðalgeirsdóttir, G., Drijfhout, S., Edwards, T., Golledge, N., Hemer, M., Kopp, R., Krinner, G., Mix, A., Notz, D., Nowicki, S., Nurhati, I., Ruiz, J., Sallée, J., Slangen, A., and Yu, Y.: Chapter 9: Ocean, Cryosphere and Sea Level Change, in: Climate Change 2021: The Physical Science Basis. Contribution of Working Group I to the Sixth Assessment Report of the Intergovernmental Panel on Climate Change, 1–257, https://doi.org/10.1017/9781009157896.011.1212, 2021.

Frederikse, T., Landerer, F., Caron, L., Adhikari, S., Parkes, D., Humphrey, V. W., Dangendorf, S., Hogarth, P., Zanna, L., Cheng, L., and Wu, Y.-H.: The causes of sea-level rise since 1900, Nature, 584, 393–397, https://doi.org/10.1038/s41586-020-2591-3, 2020.

Goelzer, H., Nowicki, S., Payne, A., Larour, E., Seroussi, H., Lipscomb, W. H., Gregory, J., Abe-Ouchi, A., Shepherd, A., Simon, E., Agosta, C., Alexander, P., Aschwanden, A., Barthel, A., Calov, R., Chambers, C., Choi, Y., Cuzzone, J., Dumas, C., Edwards, T., Felikson, D., Fettweis, X., Golledge, N. R., Greve, R., Humbert, A., Huybrechts, P., Le Clec'H, S., Lee, V., Leguy, G., Little, C., Lowry, D. P., Morlighem, M., Nias, I., Quiquet, A., Rückamp, M., Schlegel, N.-J., Slater, D. A., Smith, R. S., Straneo, F., Tarasov, L., Van De Wal, R., and Van Den Broeke, M.: The future sea-level

https://doi.org/10.5194/egusphere-2026-3874
Preprint. Discussion started: 2 September 2026

contribution of the Greenland ice sheet: a multi-model ensemble study of ISMIP6, The Cryosphere, 14, 3071–3096, https://doi.org/10.5194/tc-14-3071-2020, 2020.

Golledge, N. R., Keller, E. D., Gomez, N., Naughten, K. A., Bernales, J., Trusel, L. D., and Edwards, T. L.: Global environmental consequences of twenty-first-century ice-sheet melt, Nature, 566, 65–72, https://doi.org/10.1038/s41586-019-0889-9, 2019.

Gouretski, V. V. and Koltermann, K. P.: WOCE Global Hydrographic Climatology, Berichte Bundesamtes Für Seeschifffahrt Hydrogr., 52, 2004.

Greve, R. and Chambers, C.: Mass loss of the Greenland ice sheet until the year 3000 under a sustained late-21st-century climate, J. Glaciol., 68, 618–624, https://doi.org/10.1017/jog.2022.9, 2022.

Grinsted, A. and Christensen, J. H.: The transient sensitivity of sea level rise, Ocean Sci., 17, 181–186, https://doi.org/10.5194/os-17-181-2021, 2021.

Grinsted, A., Bamber, J., Bingham, R., Buzzard, S., Nias, I., Ng, K., and Weeks, J.: The Transient Sea Level Response to External Forcing in CMIP6 Models, Earths Future, 10, e2022EF002696, https://doi.org/10.1029/2022EF002696, 2022.

Hermans, T. H. J., Gregory, J. M., Palmer, M. D., Ringer, M. A., Katsman, C. A., and Slangen, A. B. A.: Projecting Global Mean Sea-Level Change Using CMIP6 Models, Geophys. Res. Lett., 48, https://doi.org/10.1029/2020GL092064, 2021.

Horwath, M., Gutknecht, B. D., Cazenave, A., Palanisamy, H. K., Marti, F., Marzeion, B., Paul, F., Le Bris, R., Hogg, A. E., Otosaka, I., Shepherd, A., Döll, P., Cáceres, D., Müller Schmied, H., Johannessen, J. A., Nilsen, J. E. Ø., Raj, R. P., Forsberg, R., Sandberg Sørensen, L., Barletta, V. R., Simonsen, S., Knudsen, P., Andersen, O. B., Ranndal, H., Rose, S. K., Merchant, C. J., Macintosh, C. R., Von Schuckmann, K., Novotny, K., Groh, A., Restano, M., and Benveniste, J.: ESA Sea Level Budget Closure Climate Change Initiative (SLBC_cci): Time series of global mean sea level budget and ocean mass budget elements (1993-2016, at monthly resolution), version 2.2, https://doi.org/10.5285/17C2CE31784048DE93996275EE976FFF, 2021.

Kc, S. and Lutz, W.: The human core of the shared socioeconomic pathways: Population scenarios by age, sex and level of education for all countries to 2100, Glob. Environ. Change, 42, 181–192, https://doi.org/10.1016/j.gloenvcha.2014.06.004, 2017.

Kopp, R. E., Horton, R. M., Little, C. M., Mitrovica, J. X., Oppenheimer, M., Rasmussen, D. J., Strauss, B. H., and Tebaldi, C.: Probabilistic 21st and 22nd century sea-level projections at a global network of tide-gauge sites, Earths Future, 2, 383–406, https://doi.org/10.1002/2014EF000239, 2014.

Kopp, R. E., Garner, G. G., Hermans, T. H. J., Jha, S., Kumar, P., Reedy, A., Slangen, A. B. A., Turilli, M., Edwards, T. L., Gregory, J. M., Koubbe, G., Levermann, A., Merzky, A., Nowicki, S., Palmer, M. D., and Smith, C.: The Framework for Assessing Changes To Sea-level (FACTS) v1.0: a platform for characterizing parametric and structural uncertainty in future global, relative, and extreme sea-level change, Geosci. Model Dev., 16, 7461–7489, https://doi.org/10.5194/gmd-16-7461-2023, 2023.

https://doi.org/10.5194/egusphere-2026-3874
Preprint. Discussion started: 2 September 2026

Lacroix, F., Burger, F. A., Silvy, Y., Schleussner, C., and Frölicher, T. L.: Persistently Elevated High-Latitude Ocean Temperatures and Global Sea Level Following Temporary Temperature Overshoots, Earths Future, 12, e2024EF004862, https://doi.org/10.1029/2024EF004862, 2024.

Lauvset, S. K., Key, R. M., Olsen, A., Van Heuven, S., Velo, A., Lin, X., Schirnick, C., Kozyr, A., Tanhua, T., Hoppema, M., Jutterström, S., Steinfeldt, R., Jeansson, E., Ishii, M., Perez, F. F., Suzuki, T., and Watelet, S.: A new global interior ocean mapped climatology: the 1° × 1° GLODAP version 2, Earth Syst. Sci. Data, 8, 325–340, https://doi.org/10.5194/essd-8-325-2016, 2016.

Leach, N. J., Jenkins, S., Nicholls, Z., Smith, C. J., Lynch, J., Cain, M., Walsh, T., Wu, B., Tsutsui, J., and Allen, M. R.: FaIRv2.0.0: a generalized impulse response model for climate uncertainty and future scenario exploration, Geosci. Model Dev., 14, 3007–3036, https://doi.org/10.5194/gmd-14-3007-2021, 2021.

Leloup, G., Quiquet, A., Roche, D. M., Dumas, C., and Paillard, D.: Hysteresis of the Antarctic Ice Sheet With a Coupled Climate-Ice-Sheet Model, Geophys. Res. Lett., 52, e2024GL111492, https://doi.org/10.1029/2024GL111492, 2025.

Levermann, A., Winkelmann, R., Albrecht, T., Goelzer, H., Golledge, N. R., Greve, R., Huybrechts, P., Jordan, J., Leguy, G., Martin, D., Morlighem, M., Pattyn, F., Pollard, D., Quiquet, A., Rodehacke, C., Seroussi, H., Sutter, J., Zhang, T., Van Breedam, J., Calov, R., DeConto, R., Dumas, C., Garbe, J., Gudmundsson, G. H., Hoffman, M. J., Humbert, A., Kleiner, T., Lipscomb, W. H., Meinshausen, M., Ng, E., Nowicki, S. M. J., Perego, M., Price, S. F., Saito, F., Schlegel, N.-J., Sun, S., and Van De Wal, R. S. W.: Projecting Antarctica's contribution to future sea level rise from basal ice shelf melt using linear response functions of 16 ice sheet models (LARMIP-2), Earth Syst. Dyn., 11, 35–76, https://doi.org/10.5194/esd-11-35-2020, 2020.

Levitus, S., Antonov, J. I., Boyer, T. P., Baranova, O. K., Garcia, H. E., Locarnini, R. A., Mishonov, A. V., Reagan, J. R., Seidov, D., Yarosh, E. S., and Zweng, M. M.: World ocean heat content and thermosteric sea level change (0–2000 m), 1955–2010, Geophys. Res. Lett., 39, 2012GL051106, https://doi.org/10.1029/2012GL051106, 2012.

Lorbacher, K., Nauels, A., and Meinshausen, M.: Complementing thermosteric sea level rise estimates, Geosci. Model Dev., 8, 2723–2734, https://doi.org/10.5194/gmd-8-2723-2015, 2015.

Malles, J.-H. and Marzeion, B.: Twentieth century global glacier mass change: an ensemble-based model reconstruction, The Cryosphere, 15, 3135–3157, https://doi.org/10.5194/tc-15-3135-2021, 2021.

Marti, F., Blazquez, A., Meyssignac, B., Ablain, M., Barnoud, A., Fraudeau, R., Jugier, R., Chenal, J., Larnicol, G., Pfeffer, J., Restano, M., and Benveniste, J.: Monitoring the ocean heat content change and the Earth energy imbalance from space altimetry and space gravimetry, Earth Syst. Sci. Data, 14, 229–249, https://doi.org/10.5194/essd-14-229-2022, 2022.

Martínez Montero, M., Crucifix, M., Couplet, V., Brede, N., and Botta, N.: SURFER v2.0: a flexible and simple model linking anthropogenic CO_2 emissions and solar radiation modification to ocean acidification and sea level rise, Geosci. Model Dev., 15, 8059–8084, https://doi.org/10.5194/gmd-15-8059-2022, 2022.

Marzeion, B., Jarosch, A. H., and Hofer, M.: Past and future sea-level change from the surface mass balance of glaciers, The Cryosphere, 6, 1295–1322, https://doi.org/10.5194/tc-6-1295-2012, 2012.

https://doi.org/10.5194/egusphere-2026-3874
Preprint. Discussion started: 2 September 2026

Marzeion, B., Cogley, J. G., Richter, K., and Parkes, D.: Attribution of global glacier mass loss to anthropogenic and natural causes, Science, 345, 919–921, https://doi.org/10.1126/science.1254702, 2014.

Marzeion, B., Hock, R., Anderson, B., Bliss, A., Champollion, N., Fujita, K., Huss, M., Immerzeel, W. W., Kraaijenbrink, P., Malles, J., Maussion, F., Radić, V., Rounce, D. R., Sakai, A., Shannon, S., Van De Wal, R., and Zekollari, H.: Partitioning the Uncertainty of Ensemble Projections of Global Glacier Mass Change, Earths Future, 8, e2019EF001470, https://doi.org/10.1029/2019EF001470, 2020.

Meinshausen, M., Wigley, T. M. L., and Raper, S. C. B.: Emulating atmosphere-ocean and carbon cycle models with a simpler model, MAGICC6 – Part 2: Applications, Atmospheric Chem. Phys., 11, 1457–1471, https://doi.org/10.5194/acp-11-1457-2011, 2011a.

Meinshausen, M., Raper, S. C. B., and Wigley, T. M. L.: Emulating coupled atmosphere-ocean and carbon cycle models with a simpler model, MAGICC6 – Part 1: Model description and calibration, Atmospheric Chem. Phys., 11, 1417–1456, https://doi.org/10.5194/acp-11-1417-2011, 2011b.

Meinshausen, M., Nicholls, Z. R. J., Lewis, J., Gidden, M. J., Vogel, E., Freund, M., Beyerle, U., Gessner, C., Nauels, A., Bauer, N., Canadell, J. G., Daniel, J. S., John, A., Krummel, P. B., Luderer, G., Meinshausen, N., Montzka, S. A., Rayner, P. J., Reimann, S., Smith, S. J., van den Berg, M., Velders, G. J. M., Vollmer, M. K., and Wang, R. H. J.: The shared socio-economic pathway (SSP) greenhouse gas concentrations and their extensions to 2500, Geosci. Model Dev., 13, 3571–3605, https://doi.org/10.5194/gmd-13-3571-2020, 2020.

Nauels, A., Meinshausen, M., Mengel, M., Lorbacher, K. and Wigley, T. M. L.: Synthesizing long-term sea level rise projections – the MAGICC sea level model v2.0, Geosci. Model Dev., 10, 2495–2524, 2017a.

Nauels, A., Rogelj, J., Schleussner, C.-F., Meinshausen, M., and Mengel, M.: Linking sea level rise and socioeconomic indicators under the Shared Socioeconomic Pathways, Environ. Res. Lett., 12, 114002, https://doi.org/10.1088/1748-9326/aa92b6, 2017b.

Nauels, A., Nicholls, Z., Möller, T., Hermans, T. H. J., Mengel, M., Kloenne, U., Smith, C., Slangen, A. B. A., and Palmer, M. D.: Multi-century global and regional sea-level rise commitments from cumulative greenhouse gas emissions in the coming decades, Nat. Clim. Change, 15, 1198–1204, https://doi.org/10.1038/s41558-025-02452-5, 2025.

Nauels, A., Möller, T., Couplet, V., Kopp, R., Kumar, P., Mengel, M., Munday, G., Nicholls, Z., Ramme, L., Slangen, A., Smith, C., Weeks, J., and Wong, A.: SLEIP SSP-RCP global mean sea level projections, https://doi.org/10.5281/ZENODO.21027187, 2026.

Nicholls, Z., Meinshausen, M., Lewis, J., Corradi, M. R., Dorheim, K., Gasser, T., Gieseke, R., Hope, A. P., Leach, N. J., McBride, L. A., Quilcaille, Y., Rogelj, J., Salawitch, R. J., Samset, B. H., Sandstad, M., Shiklomanov, A., Skeie, R. B., Smith, C. J., Smith, S. J., Su, X., Tsutsui, J., Vega-Westhoff, B., and Woodard, D. L.: Reduced Complexity Model Intercomparison Project Phase 2: Synthesizing Earth System Knowledge for Probabilistic Climate Projections, Earths Future, 9, e2020EF001900, https://doi.org/10.1029/2020EF001900, 2021.

https://doi.org/10.5194/egusphere-2026-3874
Preprint. Discussion started: 2 September 2026

Nicholls, Z. R. J., Meinshausen, M., Lewis, J., Gieseke, R., Dommenget, D., Dorheim, K., Fan, C.-S., Fuglestvedt, J. S., Gasser, T., Golüke, U., Goodwin, P., Hartin, C., Hope, A. P., Kriegler, E., Leach, N. J., Marchegiani, D., McBride, L. A., Quilcaille, Y., Rogelj, J., Salawitch, R. J., Samset, B. H., Sandstad, M., Shiklomanov, A. N., Skeie, R. B., Smith, C. J., Smith, S., Tanaka, K., Tsutsui, J., and Xie, Z.: Reduced Complexity Model Intercomparison Project Phase 1: introduction and evaluation of global-mean temperature response, Geosci. Model Dev., 13, 5175–5190, https://doi.org/10.5194/gmd-13-5175-2020, 2020.

Noël, B., Van Kampenhout, L., Lenaerts, J. T. M., Van De Berg, W. J., and Van Den Broeke, M. R.: A 21st Century Warming Threshold for Sustained Greenland Ice Sheet Mass Loss, Geophys. Res. Lett., 48, e2020GL090471, https://doi.org/10.1029/2020GL090471, 2021.

Palmer, M. D., Gregory, J. M., Bagge, M., Calvert, D., Hagedoorn, J. M., Howard, T., Klemann, V., Lowe, J. A., Roberts, C. D., Slangen, A. B. A., and Spada, G.: Exploring the Drivers of Global and Local Sea-Level Change Over the 21st Century and Beyond, Earths Future, 8, e2019EF001413, https://doi.org/10.1029/2019EF001413, 2020.

Pattyn, F., Ritz, C., Hanna, E., Asay-Davis, X., DeConto, R., Durand, G., Favier, L., Fettweis, X., Goelzer, H., Golledge, N. R., Kuipers Munneke, P., Lenaerts, J. T. M., Nowicki, S., Payne, A. J., Robinson, A., Seroussi, H., Trusel, L. D., and Van Den Broeke, M.: The Greenland and Antarctic ice sheets under 1.5 °C global warming, Nat. Clim. Change, 8, 1053–1061, https://doi.org/10.1038/s41558-018-0305-8, 2018.

Perrette, M. and Mengel, M.: Relative sea level projections constrained by historical trends at tide gauge sites, Sci. Adv., 11, eado4506, https://doi.org/10.1126/sciadv.ado4506, 2025.

Rahmstorf, S., Perrette, M., and Vermeer, M.: Testing the robustness of semi-empirical sea level projections, Clim. Dyn., 39, 861–875, https://doi.org/10.1007/s00382-011-1226-7, 2012.

Ramme, L., Blanz, B., Wells, C., Wong, T. E., Schoenberg, W., Smith, C., and Li, C.: Feedback-based sea level rise impact modelling for integrated assessment models with FRISIAv1.0, Geosci. Model Dev., 18, 10017–10052, https://doi.org/10.5194/gmd-18-10017-2025, 2025.

Reedy, A. and Kopp, R. E.: Temperature-Dependent Projections in FACTS v1.1.1, 2023.

Riahi, K., Van Vuuren, D. P., Kriegler, E., Edmonds, J., O'Neill, B. C., Fujimori, S., Bauer, N., Calvin, K., Dellink, R., Fricko, O., Lutz, W., Popp, A., Cuaresma, J. C., Kc, S., Leimbach, M., Jiang, L., Kram, T., Rao, S., Emmerling, J., Ebi, K., Hasegawa, T., Havlik, P., Humpenöder, F., Da Silva, L. A., Smith, S., Stehfest, E., Bosetti, V., Eom, J., Gernaat, D., Masui, T., Rogelj, J., Strefler, J., Drouet, L., Krey, V., Luderer, G., Harmsen, M., Takahashi, K., Baumstark, L., Doelman, J. C., Kainuma, M., Klimont, Z., Marangoni, G., Lotze-Campen, H., Obersteiner, M., Tabeau, A., and Tavoni, M.: The Shared Socioeconomic Pathways and their energy, land use, and greenhouse gas emissions implications: An overview, Glob. Environ. Change, 42, 153–168, https://doi.org/10.1016/j.gloenvcha.2016.05.009, 2017.

Romero-Prieto, A., Sandstad, M., Sanderson, B. M., Nicholls, Z. R. J., Steinert, N. J., Gasser, T., Mathison, C., Kikstra, J., Aubry, T. J., and Smith, C.: Reduced Complexity Model Intercomparison Project Phase 3: Experimental protocol for coordinated constraining and evaluation of Reduced-Complexity Models, https://doi.org/10.5194/egusphere-2025-5775, 21 November 2025.

Schuster, L., Maussion, F., Rounce, D. R., Ultee, L., Schmitt, P., Lacroix, F., Frölicher, T. L., and Schleussner, C.-F.: Irreversible glacier change and trough water for centuries after overshooting 1.5 °C, Nat. Clim. Change, 15, 634–641, https://doi.org/10.1038/s41558-025-02318-w, 2025.

Seroussi, H., Nowicki, S., Payne, A. J., Goelzer, H., Lipscomb, W. H., Abe-Ouchi, A., Agosta, C., Albrecht, T., Asay-Davis, X., Barthel, A., Calov, R., Cullather, R., Dumas, C., Galton-Fenzi, B. K., Gladstone, R., Golledge, N. R., Gregory, J. M., Greve, R., Hattermann, T., Hoffman, M. J., Humbert, A., Huybrechts, P., Jourdain, N. C., Kleiner, T., Larour, E., Leguy, G. R., Lowry, D. P., Little, C. M., Morlighem, M., Pattyn, F., Pelle, T., Price, S. F., Quiquet, A., Reese, R., Schlegel, N.-J., Shepherd, A., Simon, E., Smith, R. S., Straneo, F., Sun, S., Trusel, L. D., Van Breedam, J., Van De Wal, R. S. W., Winkelmann, R., Zhao, C., Zhang, T., and Zwinger, T.: ISMIP6 Antarctica: a multi-model ensemble of the Antarctic ice sheet evolution over the 21st century, The Cryosphere, 14, 3033–3070, https://doi.org/10.5194/tc-14-3033-2020, 2020.

Seroussi, H., Pelle, T., Lipscomb, W. H., Abe-Ouchi, A., Albrecht, T., Alvarez-Solas, J., Asay-Davis, X., Barre, J., Berends, C. J., Bernales, J., Blasco, J., Caillet, J., Chandler, D. M., Coulon, V., Cullather, R., Dumas, C., Galton-Fenzi, B. K., Garbe, J., Gillet-Chaulet, F., Gladstone, R., Goelzer, H., Golledge, N., Greve, R., Gudmundsson, G. H., Han, H. K., Hillebrand, T. R., Hoffman, M. J., Huybrechts, P., Jourdain, N. C., Klose, A. K., Langebroek, P. M., Leguy, G. R., Lowry, D. P., Mathiot, P., Montoya, M., Morlighem, M., Nowicki, S., Pattyn, F., Payne, A. J., Quiquet, A., Reese, R., Robinson, A., Saraste, L., Simon, E. G., Sun, S., Twarog, J. P., Trusel, L. D., Urruty, B., Van Breedam, J., Van De Wal, R. S. W., Wang, Y., Zhao, C., and Zwinger, T.: Evolution of the Antarctic Ice Sheet Over the Next Three Centuries From an ISMIP6 Model Ensemble, Earths Future, 12, https://doi.org/10.1029/2024ef004561, 2024.

Shaffer, G.: Formulation, calibration and validation of the DAIS model (version 1), a simple Antarctic ice sheet model sensitive to variations of sea level and ocean subsurface temperature, Geosci. Model Dev., 7, 1803–1818, https://doi.org/10.5194/gmd-7-1803-2014, 2014.

Smith, C. J., Forster, P. M., Allen, M., Leach, N., Millar, R. J., Passerello, G. A., and Regayre, L. A.: FAIR v1.3: a simple emissions-based impulse response and carbon cycle model, Geosci. Model Dev., 11, 2273–2297, https://doi.org/10.5194/gmd-11-2273-2018, 2018.

Smith, R. S., Bilge, T. A., Bracegirdle, T. J., Holland, P. R., Kuhlbrodt, T., Lang, C., Liddicoat, S., Mitcham, T., Mulcahy, J., Naughten, K. A., Orr, A., Palmieri, J., Payne, A. J., Rumbold, S., Stringer, M., Swaminathan, R., Taylor, S., Walton, J., and Jones, C.: Response of ice sheets, sea-ice and sea level in climate stabilisation and reversibility simulations using a state-of-the-art Earth System Model, Earth Syst. Dyn., 17, 475–493, https://doi.org/10.5194/esd-17-475-2026, 2026.

Turner, F. E., Malagon Santos, V., Edwards, T. L., Slangen, A. B. A., Nicholls, R. J., Le Cozannet, G., O'Neill, J., and Adhikari, M.: Illustrative Multi-Centennial Projections of Global Mean Sea-Level Rise and Their Application, Earths Future, 11, e2023EF003550, https://doi.org/10.1029/2023EF003550, 2023.

https://doi.org/10.5194/egusphere-2026-3874
Preprint. Discussion started: 2 September 2026

Vega-Westhoff, B., Sriver, R. L., Hartin, C. A., Wong, T. E., and Keller, K.: Impacts of Observational Constraints Related to Sea Level on Estimates of Climate Sensitivity, Earths Future, 7, 677–690, https://doi.org/10.1029/2018EF001082, 2019.

Weaver, A. J., Eby, M., Wiebe, E. C., Bitz, C. M., Duffy, P. B., Ewen, T. L., Fanning, A. F., Holland, M. M., MacFadyen, A., Matthews, H. D., Meissner, K. J., Saenko, O., Schmittner, A., Wang, H., and Yoshimori, M.: The UVic earth system climate model: Model description, climatology, and applications to past, present and future climates, Atmosphere-Ocean, 39, 361–428, https://doi.org/10.1080/07055900.2001.9649686, 2001.

Weeks, J. H., Fung, F., Harrison, B. J., and Palmer, M. D.: The evolution of UK sea-level projections, Environ. Res. Commun., 5, 032001, https://doi.org/10.1088/2515-7620/acc020, 2023.

Wigley, T. M. L. and Raper, S. C. B.: Extended scenarios for glacier melt due to anthropogenic forcing, Geophys. Res. Lett., 32, 2004GL021238, https://doi.org/10.1029/2004GL021238, 2005.

Winkelmann, R. and Levermann, A.: Linear response functions to project contributions to future sea level, Clim. Dyn., 40, 2579–2588, https://doi.org/10.1007/s00382-012-1471-4, 2013.

Wong, T.: Modeling the Sea-Level Change from U.S. Vehicle Emissions, 2026.

Wong, T., Rennels, L., Errickson, F., Srikrishnan, V., Bakker, A., Keller, K., and Anthoff, D.: Model Output Supporting MimiBRICK v2.0.0, , https://doi.org/10.5281/zenodo.20592337, 2026.

Wong, T. E., Bakker, A. M. R., Ruckert, K., Applegate, P., Slangen, A. B. A., and Keller, K.: BRICK v0.2, a simple, accessible, and transparent model framework for climate and regional sea-level projections, Geosci. Model Dev., 10, 2741–2760, https://doi.org/10.5194/gmd-10-2741-2017, 2017a.

Wong, T. E., Bakker, A. M. R., and Keller, K.: Impacts of Antarctic fast dynamics on sea-level projections and coastal flood defense, Clim. Change, 144, 347–364, https://doi.org/10.1007/s10584-017-2039-4, 2017b.

Wong, T. E., Rennels, L., Errickson, F., Srikrishnan, V., Bakker, A., Keller, K., and Anthoff, D.: MimiBRICK.jl: A Julia package for the BRICK model forsea-level change in the Mimi integrated modeling framework, J. Open Source Softw., 7, 4556, https://doi.org/10.21105/joss.04556, 2022a.

Wong, T. E., Ledna, C., Rennels, L., Sheets, H., Errickson, F. C., Diaz, D., and Anthoff, D.: Sea Level and Socioeconomic Uncertainty Drives High-End Coastal Adaptation Costs, Earths Future, 10, e2022EF003061, https://doi.org/10.1029/2022EF003061, 2022b.

Zemp, M., Huss, M., Thibert, E., Eckert, N., McNabb, R., Huber, J., Barandun, M., Machguth, H., Nussbaumer, S. U., Gärtner-Roer, I., Thomson, L., Paul, F., Maussion, F., Kutuzov, S., and Cogley, J. G.: Global glacier mass changes and their contributions to sea-level rise from 1961 to 2016, Nature, 568, 382–386, https://doi.org/10.1038/s41586-019-1071-0, 2019.